



ARTICLE

SMGL-1/NBAS acts as a RAB-8 GEF to regulate unconventional protein secretion

Xianghong Wang¹, Xinxin Li¹, Junkai Wang¹, Jiabin Wang¹, Can Hu¹, Jia Zeng³, Anbing Shi^{1,2} , and Long Lin^{1,2} 

Unconventional protein secretion (UPS) pathways are conserved across species. However, the underlying mechanisms that regulate Golgi-bypassing UPS of integral proteins remain elusive. In this study, we show that RAB-8 and SMGL-1/NBAS are required for the UPS of integral proteins in *C. elegans* intestine. SMGL-1 resides in the ER-Golgi intermediate compartment and adjacent RAB-8-positive structures, and NRZ complex component CZW-1/ZW10 is required for this residency. Notably, SMGL-1 acts as a guanine nucleotide exchange factor for RAB-8, ensuring UPS of integral proteins by driving the activation of RAB-8. Furthermore, we show that *Pseudomonas aeruginosa* infection elevated the expression of SMGL-1 and RAB-8. Loss of SMGL-1 or RAB-8 compromised resistance to environmental colchicine, arsenite, and pathogenic bacteria. These results suggest that the SMGL-1/RAB-8-mediated UPS could integrate environmental signals to serve as a host defense response. Together, by establishing the *C. elegans* intestine as a multicellular model, our findings provide insights into RAB-8-dependent Golgi-bypassing UPS, especially in the context of epithelia in vivo.

Introduction

Unconventional protein secretion (UPS) refers to secretory pathways by which proteins bypass the ER-Golgi before being exported to the plasma membrane or extracellular space (Giuliani et al., 2011; Zhang and Schekman, 2013; Rabouille, 2017). Recent evidence has demonstrated that the dysregulation of UPS is associated with pathologies for several human diseases, ranging from neurodegeneration to cancers (Ejlertskov et al., 2013; Malhotra, 2013; Lock et al., 2014; Son et al., 2016; Rabouille, 2017; Dimou and Nickel, 2018; Kim et al., 2018). There are at least four UPS pathways that fall into two major categories (Rabouille, 2017; Dimou and Nickel, 2018). The first category comprises Type I-III UPS, involving soluble proteins lacking the signal peptides that direct them into the ER (ER-Golgi bypassing). The second category (Type IV) mainly refers to the UPS of transmembrane proteins inserted into the ER membrane, bypassing the Golgi while traveling to the cell surface (Rabouille, 2017; Dimou and Nickel, 2018).

The physiological significance of Type IV UPS is gradually being appreciated (Yoo et al., 2002; Gee et al., 2011; Jung et al., 2016; Gee et al., 2018; Park et al., 2020). The prominent cargoes of Type IV UPS include mutant proteins cystic fibrosis transmembrane conductance regulator (CFTR/ABCC7) and pendrin, the functional deficiency of which is related to cystic fibrosis and

Pendred syndrome, respectively (Gee et al., 2011; Jung et al., 2016; Park et al., 2020). In addition, non-mutant proteins integrin, polycystin 2, and peripherin have also been reported to reach the plasma membrane or cilia bypassing the Golgi (Schotman et al., 2008; Hoffmeister et al., 2011; Gee et al., 2011; Tian et al., 2014; Jung et al., 2016; Park et al., 2020). Notably, several studies have shown divergence in the regulatory mechanisms controlling Type IV UPS. For example, Golgi re-assembly stacking protein (GRASP) plays a role in the secretion of mutant CFTR and α integrin but does not regulate the UPS of mutant pendrin and cilia peripherin (Schotman et al., 2008; Gee et al., 2011; Tian et al., 2014; Jung et al., 2016).

UPS pathways are conserved across species, mostly non-constitutive and triggered by stress events, including inflammation, starvation, and mechanical stress (Giuliani et al., 2011; Rabouille et al., 2012; Malhotra, 2013; Rabouille, 2017; Kim et al., 2018; Gee et al., 2018; Dimou and Nickel, 2018). For example, the UPS of mutant CFTR and pendrin is induced by the blockage of conventional ER-to-Golgi pathway or ER stress (Gee et al., 2011; Jung et al., 2016). Given that more UPS cargoes are being identified, the existence of a constitutive steady-state UPS and its potential physiological roles remain to be clarified. It is noteworthy that the transit of integral membrane proteins from the

¹Department of Biochemistry and Molecular Biology, School of Basic Medicine, Tongji Medical College, Huazhong University of Science and Technology, Wuhan, Hubei, China; ²Cell Architecture Research Center, Huazhong University of Science and Technology, Wuhan, Hubei, China; ³Department of Biochemistry and Molecular Biology, Guizhou Medical University, Guiyang, Guizhou, China.

Correspondence to Anbing Shi: ashi@hust.edu.cn; Long Lin: longlin@hust.edu.cn.

© 2022 Wang et al. This article is distributed under the terms of an Attribution-Noncommercial-Share Alike-No Mirror Sites license for the first six months after the publication date (see <http://www.rupress.org/terms/>). After six months it is available under a Creative Commons License (Attribution-Noncommercial-Share Alike 4.0 International license, as described at <https://creativecommons.org/licenses/by-nc-sa/4.0/>).

ER to the Golgi apparatus is a rate-limiting step (Schröder and Kaufman, 2005). The steady-state UPS pathway could step in to improve the secretion efficiency of integral membrane proteins, thus responding to environmental pressures effectively. In this respect, in addition to *Drosophila* epithelial cells (Schotman et al., 2008), the significance of the study on UPS pathways in a live animal model is getting appreciated.

The plasma membrane of epithelia is partitioned into apical and basolateral domains to mediate communication with the external environment and neighboring cells, respectively (Caplan, 1997; Nelson and Yeaman, 2001). In epithelial cells, the trans-Golgi network (TGN) functions as the primary sorting organelle for newly synthesized proteins destined for the apical domain (Fuller et al., 1985; Harada, 2010). However, it is unclear how Type IV UPS cargoes bypass the Golgi in epithelia, particularly given the apical localization of proteins such as CFTR. Furthermore, epithelial cells contain distinct apical and basolateral classes of endosomes (Sheff et al., 2002; Folsch et al., 2009). While endosomes have been implicated in conventional apical secretion (Cresawn et al., 2007; Thuenauer et al., 2014), it remains unclear whether endosomal compartments also participate in Golgi-bypassing Type IV UPS. In this study, we identified SMGL-1, a homolog of NBAS (neuroblastoma amplified sequence), as a RAB-8 GEF. Loss of SMGL-1 impaired the UPS of a subset of apical integral proteins in intestinal epithelia. In *C. elegans*, PGPs provide a protective mechanism against environmental stressors, such as natural toxins, heavy metals, and pathogens (Broeks et al., 1995; Broeks et al., 1996; Mahajan-Miklos et al., 1999). Notably, overaccumulated PGP-1 in *rab-8* or *smgl-1* mutants was partially located in PI3P-positive membrane structures. Consistent with these findings, SMGL-1 and RAB-8 are both required for resistance to pathogenic bacteria and exposure to colchicine or arsenite. Furthermore, we noticed that *P. aeruginosa* treatment promoted the level of SMGL-1 and RAB-8, suggesting that the SMGL-1/RAB-8-mediated UPS pathway could be regulated by infection-related conditions. Altogether, our study establishes the *C. elegans* intestine as a multicellular model and provides insights into the mechanisms and physiological significance of RAB-8-dependent Type IV UPS.

Results

Loss of SMGL-1 impairs apical secretion in a cargo-selective manner

Recent studies in model systems indicated that RAB-8/Rab8 modulates apical exocytosis in epithelial cells (Sato et al., 2007; Vogel et al., 2015). In particular, Rab8 has been suggested to underlie the secretory transport of UPS cargos polycystin-2 and mutant CFTR (Hoffmeister et al., 2011; Noh et al., 2018). In *C. elegans*, the concurrent loss of RAB-8 and its closest paralog, RAB-10, leads to sterility, although *rab-10* mutants are viable and superficially normal in growth and development (Shi et al., 2010; Wang et al., 2016). To identify proteins that regulate RAB-8 in *C. elegans*, we performed a genome-wide synthetic sterility screen (19763 RNAi clones) in a *rab-10(ok1494)* mutant background. Using RNAi vector L4440 as a negative control and *rab-8(RNAi)* as a positive control, we focused on the synthetic

sterility (embryonic lethality and/or larval arrest) induced by the concomitant loss of RAB-10 and candidate RAB-8 regulators. After excluding those candidates with insignificant phenotypes in subsequent validation, a total of 39 candidates were obtained, including three worm-specific genes, four nuclear proteins, 18 regulators involved in protein and nucleic acid synthesis and stability, one kinase and one ubiquitin ligase, two metabolic regulators, 10 membrane trafficking and cytoskeleton-related proteins.

In *C. elegans*, previous experiments have revealed that the localization and morphology of apical endosomes were impaired in epithelial cells depleted of the candidate protein SMGL-1 (Winter et al., 2012). Accordingly, we decided to assess the mechanism by which SMGL-1 serves as a putative regulator of RAB-8. SMGL-1 (*smg lethal*) is homologous to mammalian NBAS and belongs to the SMG family of core NMD (nonsense-mediated mRNA decay) factors (Longman et al., 2007; Longman et al., 2013). Conserved domain prediction indicated that SMGL-1 harbors an N-terminal WD40 repeat domain and C-terminal α -helices (Fig. 1 A). To circumvent the embryonic lethality and/or sterility of *smgl-1* null mutants (Longman et al., 2007), we constructed a transgenic allele *smgl-1(ycxEx1659)*, a heat-shock-inducible CRISPR/Cas9 conditional mutant (Fig. 1 A).

We first examined the secretion phenotypes in SMGL-1-deficient animals. P-glycoproteins (PGPs) are members of the ABC transporter family (subfamily B; Sheps et al., 2004). RAB-8 has been shown to regulate the apical secretion of PGP-1/ABCBI in the intestine of *C. elegans* (Sato et al., 2007; Vogel et al., 2015). As expected, we observed that GFP-tagged PGP-1 was predominantly localized to the apical membrane and accumulated in the intracellular structures of *rab-8(tm2526)* (Figs. 1, B and D; and S1 A; Sato et al., 2007). Similarly, SMGL-1 deficiency resulted in the intracellular accumulation of GFP::PGP-1 in L4 larvae and day-1 adults without enhancing the protein level of PGP-1 (Figs. 1, C-F; and S1, A-C). Overexpression of the CRISPR/Cas9-editing resistant variant of SMGL-1 effectively rescued this phenotype in *smgl-1(ycxEx1659)* mutants (Fig. 1, C and D), indicating that impaired secretion of PGP-1 can be attributed to the loss of SMGL-1. In contrast, the loss of RAB-10, the closest paralog of RAB-8, did not affect the distribution of GFP::PGP-1 (Fig. 1, C and D). Likewise, the distributional defects of PGP-1 in *smgl-1* mutants were not further exacerbated by simultaneous loss of RAB-10 (Fig. S1 D). Taken together, these observations demonstrated that SMGL-1 also plays a role in apical exocytosis of PGP-1 in the intestinal epithelia. Of note, we did not observe a decrease in GFP::PGP-1 in the apical membrane in *rab-8* and *smgl-1* mutants, most likely because overexpression of the transgenic GFP::PGP-1 overwhelmed this putative reduction.

We then tested the fate of accumulated GFP::PGP-1 in *smgl-1* mutants by performing colocalization assays with a set of organelle markers. In the absence of SMGL-1, GFP::PGP-1 did not colocalize with Golgi markers AMAN-2::RFP (*cis*- and *medial*-Golgi cisternae), mCherry::GOLG-4 (TGN), and mCherry::APG-1 (TGN) (Fig. S1 E), indicating that PGP-1 did not accumulate in Golgi apparatus. Phosphoinositide PI3P is required for various cellular processes, including retrograde transport from endosomes, multivesicular body sorting, autophagy, and vesicle

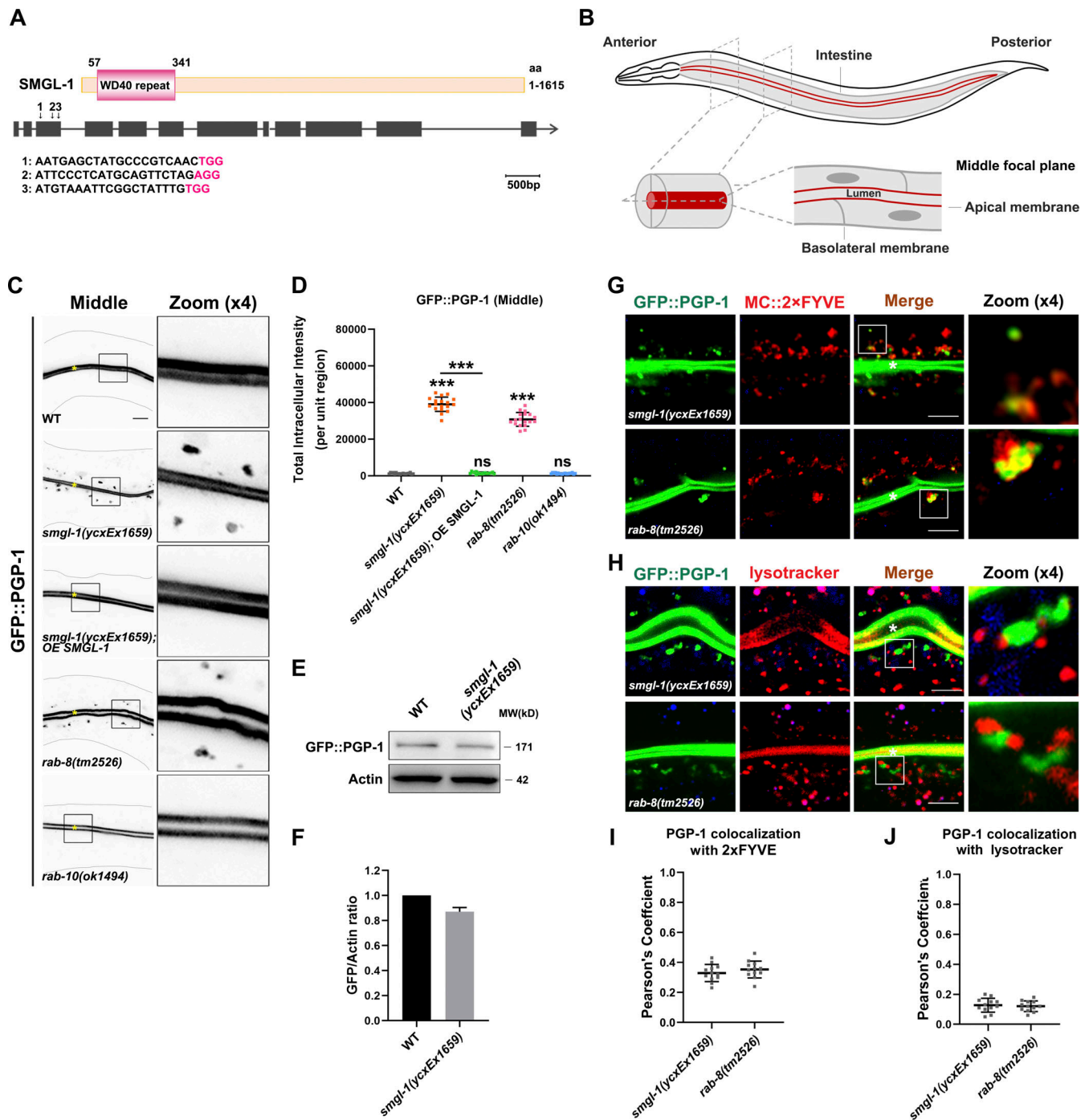


Figure 1. Loss of SMGL-1 impairs apical secretion of PGP-1. (A) Domain architecture of SMGL-1. SMGL-1 contains the N-terminal WD40 repeats domain, while amino acid numbers are indicated. *smgl-1* open reading frame and the corresponding sequence changes of *smgl-1(ycxEx1659)*, a heat-shock-inducible CRISPR/Cas9 conditional mutant, are indicated. Arrowheads show three single guide RNAs target locations. (B) A diagram of *C. elegans* intestine, showing the apical and basolateral membranes. The imaging plane where the apical membrane and intestinal lumen can be observed is defined as the middle focal plane of the confocal microscopy. (C and D) Confocal images of intestinal cells expressing GFP-tagged PGP-1. GFP::PGP-1 is explicitly localized in the apical membrane of intestinal epithelia in L4 larvae of wild-type animals and *rab-10(ok1494)* mutants. In contrast, GFP::PGP-1 displayed intracellular accumulation in *smgl-1(ycxEx1659)* and *rab-8(tm2526)* mutants. Overexpression of CRISPR/Cas9-editing resistant SMGL-1 rescued the localization defects of PGP-1 in *smgl-1(ycxEx1659)* mutants. The signals from the apical membrane were avoided by manual ROI selection. Data are shown as mean \pm SD ($n = 18$ each, six animals of each genotype sampled in three different unit regions of each intestine defined by a 100×100 [pixel²] box positioned at random). Statistical significance was determined using a one-way ANOVA followed by a post-hoc test (Dunn's Multiple Comparison Test) for multiple comparisons. ***, $P < 0.001$. Data distribution was assumed to be normal but this was not formally tested. (E and F) Western blot showing expressional levels of GFP::PGP-1 in wild-type animals and *smgl-1(ycxEx1659)* mutant. (G and H) Confocal images showing colocalization between PGP-1 and organelle markers in the intestinal cells. GFP::PGP-1 partially overlapped with PI(3)P sensor 2xFYVE in *smgl-1(ycxEx1659)* and *rab-8(tm2526)* mutants. However, GFP::PGP-1 puncta were separated from Lysotracker-labeled lysosomes in *smgl-1(ycxEx1659)* and *rab-8(tm2526)* mutants. (I and J) Quantification of colocalization of PGP-1 with 2xFYVE and Lysotracker in *smgl-1(ycxEx1659)*

and *rab-8(tm2526)* mutants. Pearson's correlation coefficients for GFP and mCherry signals were calculated ($n = 12$ animals). The signals from the apical membrane were avoided by manual ROI selection. Scale bars: 10 μm . Colored asterisks indicate intestinal lumen. A dotted line indicates the outline of the intestine. Source data are available for this figure: SourceData F1.

fusion, and can serve as a marker for intracellular membrane compartments (Steinfeld et al., 2021). Interestingly, we noticed that overaccumulated GFP::PGP-1 overlapped with a subset of mCherry::2xFYVE-labeled PI3P structures following the SMGL-1 or RAB-8 knockout (Fig. 1, G and I). The previous studies reported that apical proteins, including DPPIV, ALP, SI, PepT1, and APN, enter late endosome/lysosome after the secretory blockage in the small intestine of Rab8-deficient mice (Sato et al., 2007; Sato et al., 2014a). However, we did not observe a significant overlap between GFP::PGP-1 and lysotracker-labeled lysosomes in *rab-8(tm2526)* or *smgl-1(ycxEx1659)* mutants (Fig. 1, H and J). Taken together, our results suggested that SMGL-1 deficiency could lead to the accumulation of a fraction of PGP-1 in PI3P-enriched membranous structures without undergoing lysosome-mediated degradation.

To define the functional specificity of SMGL-1 during intestinal secretion, we assayed additional apical integral and peripheral membrane proteins, including PEPT-1 (oligopeptide transporter), SID-2 (dsRNA receptor), NHX-2 (Na^+/H^+ exchanger), ERM-1 (membrane-cytoskeleton linker), and ACT-5/actin (Nehrke, 2003; Mcewan et al., 2012; Gobel et al., 2004; Macqueen et al., 2005). PEPT-1::GFP and SID-2::GFP displayed intracellular accumulation in *smgl-1(ycxEx1659)* mutants (Fig. S1, F and G). However, SMGL-1 knockout showed no effects on the distribution of NHX-2::GFP, ERM-1::GFP or ACT-5::GFP (Fig. S1, I–K), which suggests that SMGL-1 regulates the secretion of apical integral proteins in a cargo-selective manner. We also examined whether SMGL-1 deficiency affected the localization of basolateral secretory cargoes SLCF-1::GFP (monocarboxylate transporter) and NPY::GFP (neuropeptide Y; Nagai et al., 2002; Mouchiroud et al., 2011). Nevertheless, the distribution of SLCF-1::GFP or NPY::GFP was not affected in *smgl-1(ycxEx1659)* mutants (Fig. S1, L and M). It is worth noting that although RAB-8 deficiency led to the aberrant localization of all apical cargo proteins, it did not disturb the distribution of the basolateral cargo SLCF-1::GFP (Fig. S1, F and G; and I–L). This phenotypic discrepancy between RAB-8- and SMGL-1-deficient animals suggested that while SMGL-1 and RAB-8 act in concert during the exocytosis of a set of apical proteins, RAB-8 performs additional SMGL-1-independent functions in apical secretion.

SMGL-1 is implicated in the Golgi-bypassing unconventional secretion

Thus far, our evidence has demonstrated that SMGL-1 regulates the secretion of a subset of apical integral proteins. In particular, intracellular PGP-1 accumulation did not overlap with Golgi markers in SMGL-1-deficient cells (Fig. S1 E). These findings prompted us to discriminate the itinerary of these particular cargoes. BFA (brefeldin A) has been shown to disrupt the integrity of Golgi and inhibit the early processes required for conventional secretion (Klausner et al., 1992). Accordingly, the microinjection of BFA into the intestine resulted in AMAN-2

redistribution from the Golgi to the patch structural remnants (Fig. S1 H). However, GFP::PGP-1 and PEPT-1::GFP showed no aberrations in their distribution following BFA microinjection compared to *smgl-1(ycxEx1659)* mutants (Fig. 2, A–D), suggesting that SMGL-1 is implicated in the apical secretory route bypassing the Golgi apparatus. Supporting this notion, the properly localized NHX-2, ERM-1, and ACT-5 in *smgl-1* mutants exhibited intracellular accumulation and/or basolateral mislocalization following BFA treatment (Fig. S1, I–K). Conventional Golgi-mediated sorting directs exocytosis of both apical and basolateral cargoes. We further ascertained the efficacy of BFA treatment by observing the absence of the tubular distribution of the basolateral secretory protein SLCF-1::GFP (Fig. S1 L). By employing a series of organelle markers, including GOLG-4-labeled TGN, RAB-5-labeled early endosomes, 2xFYVE-labeled PI3P-positive structures, and lysotracker-labeled mature lysosomes, we observed that enlarged NHX-2 structures partially overlapped with the lysotracker-labeled lysosome (Fig. 3, A and B). In contrast, ERM-1 and ACT-5 puncta did not colocalize with GOLG-4, RAB-5, 2xFYVE, or lysotracker (Fig. 3, C–F). Together, these data suggested that when the ER-Golgi secretory pathway was blocked, NHX-2, ERM-1, and ACT-5 were accumulated in various intracellular structures, and some NHX-2 entered the degradation route. It is noteworthy that SID-2::GFP accumulated in punctate structures in both *smgl-1* mutants and BFA-treated animals (Figs. 2, E and F; and S1 G), indicating that SID-2 could be exocytosed via both conventional ER-to-Golgi and Golgi-bypassing routes.

To corroborate the results of BFA treatment, we further used tyrphostin AG1478 to impair Golgi structure without disturbing endosomes (Pan et al., 2008; Boncompain et al., 2019). Similarly, after AG1478 microinjection, GFP::PGP-1 and PEPT-1::GFP localization did not differ from that of untreated worms, while the distributions of GFP-tagged SID-2, NHX-2, ERM-1, ACT-5, and SLCF-1 were disrupted (Figs. 2, A–F and S1, I–L). Together, these data suggested that PGP-1 and PEPT-1 could bypass Golgi en route to the apical membrane, and SMGL-1 is required for this process.

Endo H (endoglycosidase H) primarily cleaves high mannose oligosaccharides from N-linked glycoproteins, and PNGase F (Peptide-N-Glycosidase F) removes almost all N-linked oligosaccharides from glycoproteins. We sought to affirm the Golgi-bypassing secretion route of PGP-1 by testing its sensitivity to Endo H and PNGase F. If PGP-1 transits the ER en route to the TGN, it will acquire Endo H resistance through an ordered series of complex N-glycosylation events. However, FLAG::PGP-1 was sensitive to both Endo H and PNGase F treatments, yielding a lower molecular weight band (Fig. 2 G). Likewise, an ER-resident glycoprotein CNX-1/Calnexin (positive control) displayed Endo H sensitivity (Fig. 2 G). We further tested the sensitivity of SID-2 (Fig. S1 G'), which was suggested to be exocytosed via both ER-to-Golgi and Golgi-bypassing routes. Similarly, after Endo H treatment, we observed a lower

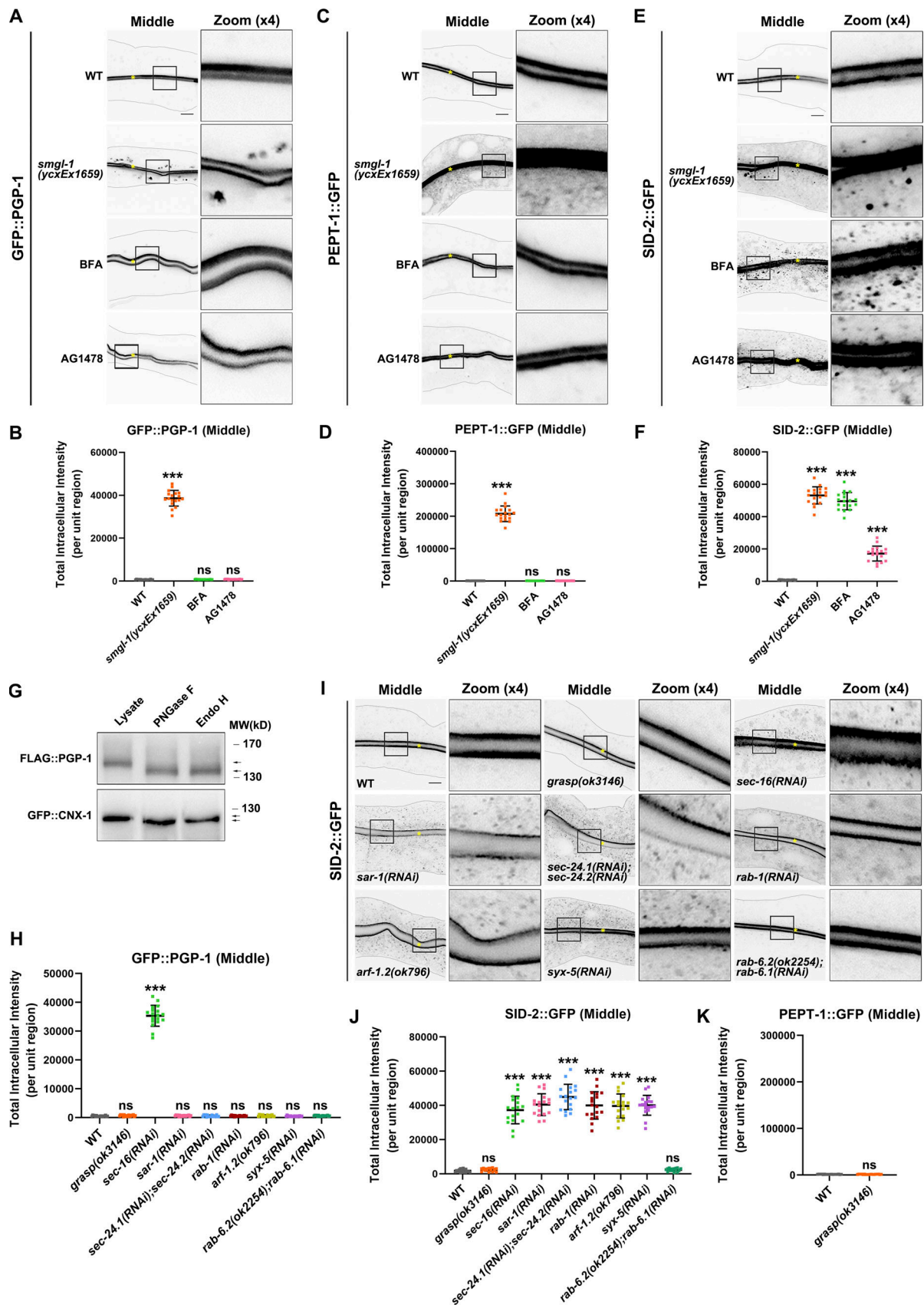


Figure 2. **SMGL-1 regulates the Golgi-bypassing unconventional secretion of apical integral proteins.** (A–D) Confocal images of intestinal cells expressing GFP-tagged PGP-1 (A and B) and PEPT-1 (C and D). Compared with wild-type animals, *smgl-1(ycxEx1659)* mutants displayed intracellular accumulation of GFP::PGP-1 and PEPT-1::GFP. In contrast, BFA and AG1478 treatment did not affect the apical localization of GFP::PGP-1 and PEPT-1::GFP. (E and F) Confocal

images of intestinal cells expressing GFP-tagged SID-2. Compared with wild-type animals, *smgl-1(yxcEx1659)* mutants displayed intracellular accumulation of SID-2::GFP. BFA and AG1478 treatment also caused intracellular accumulation of SID-2::GFP. **(G)** FLAG::PGP-1 and GFP::CNX-1 transgenic animals were analyzed by immunoblotting using anti-FLAG and anti-GFP antibodies after Endo H or PNGase F treatment. The molecular weight of FLAG::PGP-1 and GFP::CNX-1 is decreased (lower arrow) after Endo H treatment, compared with control animals (upper arrow). CNX-1, a *C. elegans* homolog of Calnexin, is an ER-resident glycoprotein and Endo H sensitive. Thus, CNX-1 was deployed as a positive control of Endo H treatment. **(H)** The apical localization of GFP::PGP-1 did not change in animals deficient in GRASP, SAR-1/Sar1, SEC-24.1/Sec24C/Sec24D and SEC-24.2/Sec24A/Sec24B, RAB-1/Rab1, ARF-1.2/Arf1, SYX-5/Stx5, RAB-6.1 and RAB-6.2. In contrast, SEC-16/Sec16 knockdown caused intracellular accumulation of GFP::PGP-1. **(I and J)** Confocal images of intestinal cells expressing GFP-tagged SID-2. The apical localization of SID-2::GFP did not change in animals deficient in GRASP or RAB-6.1 and RAB-6.2. However, SID-2::GFP displayed abnormal localization in animals deficient in SEC-16/Sec16, SAR-1/Sar1, SEC-24.1/Sec24C/Sec24D and SEC-24.2/Sec24A/Sec24B, RAB-1/Rab1, ARF-1.2/Arf1, and SYX-5/Stx5. **(K)** GRASP knockdown did not cause intracellular accumulation of PEPT-1::GFP. The signals from the apical membrane were avoided by manual ROI selection. Data are shown as mean \pm SD ($n = 18$ each, six animals of each genotype sampled in three different unit regions of each intestine defined by a 100×100 [pixel²] box positioned at random). Statistical significance was determined using a two-tailed, unpaired Student's *t* test. For multiple comparisons, statistical significance was determined using a one-way ANOVA followed by a post-hoc test (Dunn's Multiple Comparison Test). ***, $P < 0.001$. Data distribution was assumed to be normal, but this was not formally tested. Scale bars: 10 μ m. Colored asterisks indicate intestinal lumen. A dotted line indicates the outline of the intestine. Source data are available for this figure: SourceData F2.

molecular weight band (red arrow). In contrast, high molecular weight smear still existed (black arrow), which might correspond to other types of glycosylation. Taken together, these results affirmed the validity of the experiments and consolidated that PGP-1 is exocytosed via the Golgi-bypassing route.

COP II-coated vesicles are the primary carriers of mediating export from the ER. In this process, two layers of coat proteins, the Sec23/24 inner layer and the Sec13/31 outer layer, are recruited by active Sar1-GTPase at specific ER exit sites (ERES) marked by Sec16 (Lee et al., 2004). We then examined the effects of the regulators that participate in COPII coat formation and early secretion steps. Accordingly, we assayed two distinct types of apical cargoes, GFP::PGP-1 and SID-2::GFP. Notably, GFP::PGP-1 did not display intracellular accumulation in animals deficient in SAR-1/Sar1, SEC-24.1/Sec24C/Sec24D and SEC-24.2/Sec24A/Sec24B, ARF-1.2/Arf1, RAB-1/Rab1, or SYX-5/Stx5 (Fig. 2 H). In contrast, SEC-16/Sec16 knockdown caused abnormal cytosolic accumulation of PGP-1 (Fig. 2 H). In agreement with this observation, a recent study showed that the depletion of COP II components (Sar1, Sec23, Sec24, Sec13, and Sec31) did not disturb the Type IV UPS of mutant CFTR, whereas the loss of Sec16A did (Piao et al., 2017). SID-2, which likely reaches the apical surface via both the conventional and non-conventional secretory pathways, showed abnormal localization in all mutants (Fig. 2, I and J). Rab6 is a Golgi- and endosome-localized regulator of post-Golgi transport (Fourriere et al., 2019). The concurrent loss of RAB-6.1 and RAB-6.2 failed to affect either GFP::PGP-1 or SID-2::GFP distribution (Fig. 2, H–J). Together, these findings suggested that apical Type IV UPS might not require COP II, and SEC-16/Sec16, by an as yet to be determined mechanism, functions independently of other core COP II components during the Type IV UPS.

GRASP has been implicated in the unconventional secretion of mutant CFTR/ABCC7 and integrin (Schotman et al., 2008; Gee et al., 2011; Kim et al., 2016). *C. elegans* genome encodes one GRASP counterpart, Y42H9AR.1. We also tested the involvement of GRASP in Type IV UPS. However, GRASP knockdown did not cause intracellular accumulation of GFP::PGP-1 (Fig. 2 H). Consistently, the subcellular distribution of neither PEPT-1 nor SID-2 was affected (Fig. 2, I–K). Hence, we concluded that GRASP acts differently in *C. elegans* intestinal epithelia than in *Drosophila* follicular epithelial cells, substantiating the diversity

and heterogeneity of unconventional secretion pathways (Rabouille, 2017).

SMGL-1 acts as a guanine nucleotide exchange factor for RAB-8

Our genome-wide RNAi screen identified SMGL-1 as a putative regulator of RAB-8. Consistent with this perception, we observed that the lack of RAB-8 or SMGL-1 resulted in a similar intracellular accumulation phenotype of Type IV UPS cargoes. To gain insight into the mechanism by which SMGL-1 functions in the RAB-8-dependent UPS, we examined the effect of SMGL-1 knockdown on the localization of RAB-8. In *C. elegans* intestinal epithelia, low-copy transgenic GFP::RAB-8 labels punctate structures (Fig. 4 A), which are likely post-Golgi carriers and/or endosomes (Roland et al., 2007; Hattula et al., 2006; Grigoriev et al., 2011; Shi et al., 2010). In L4 larvae and day-1 adults, GFP::RAB-8 lost its punctate labeling and appeared diffusive in the cytoplasm of SMGL-1-deficient cells (Figs. 4, A and B; and S2, A and B), which was unlikely due to the NMD effects of SMGL-1 (Fig. S2, C and D). Ectopic expression of a CRISPR/Cas9-editing resistant variant of SMGL-1 restored the punctate distribution of GFP::RAB-8 (Fig. 4, A and B), suggesting that SMGL-1 functions cell autonomously in the intestinal cells to promote proper RAB-8 localization. To evaluate whether the dispersed distribution of RAB-8 is due to impaired endosomal association, we performed membrane fractionation assays. Our results showed that the ratio of membrane-to-cytosolic (P/S) GFP::RAB-8 decreased dramatically in *smgl-1(yxcEx1659)* animals (Fig. 4 C). In contrast, the ratio of membrane-to-cytosolic GFP::RAB-5 (early endosome marker) or GFP::RAB-7 (late endosome marker) was unaffected by SMGL-1 knockout (Figs. 4 C and S2 G). Consistently, the distribution of GFP::RAB-5 remained intact in *smgl-1* mutants (Fig. S2, E and F).

Inactive Rabs typically remain cytosolic in a GDI-bound state. The subcellular distribution of Rabs serves as an indicator of GEF-mediated activation (Blumer et al., 2013; Liu et al., 2018). Given that the loss of SMGL-1 resulted in impaired GFP::RAB-8 membrane association, we reasoned that SMGL-1 could function as a RAB-8 GEF. Consistent with this possibility, co-immunoprecipitation assays demonstrated that SMGL-1 could bind to RAB-8 (Fig. S2 H). In particular, SMGL-1 preferentially interacted with the inactive RAB-8(T22N) rather than the

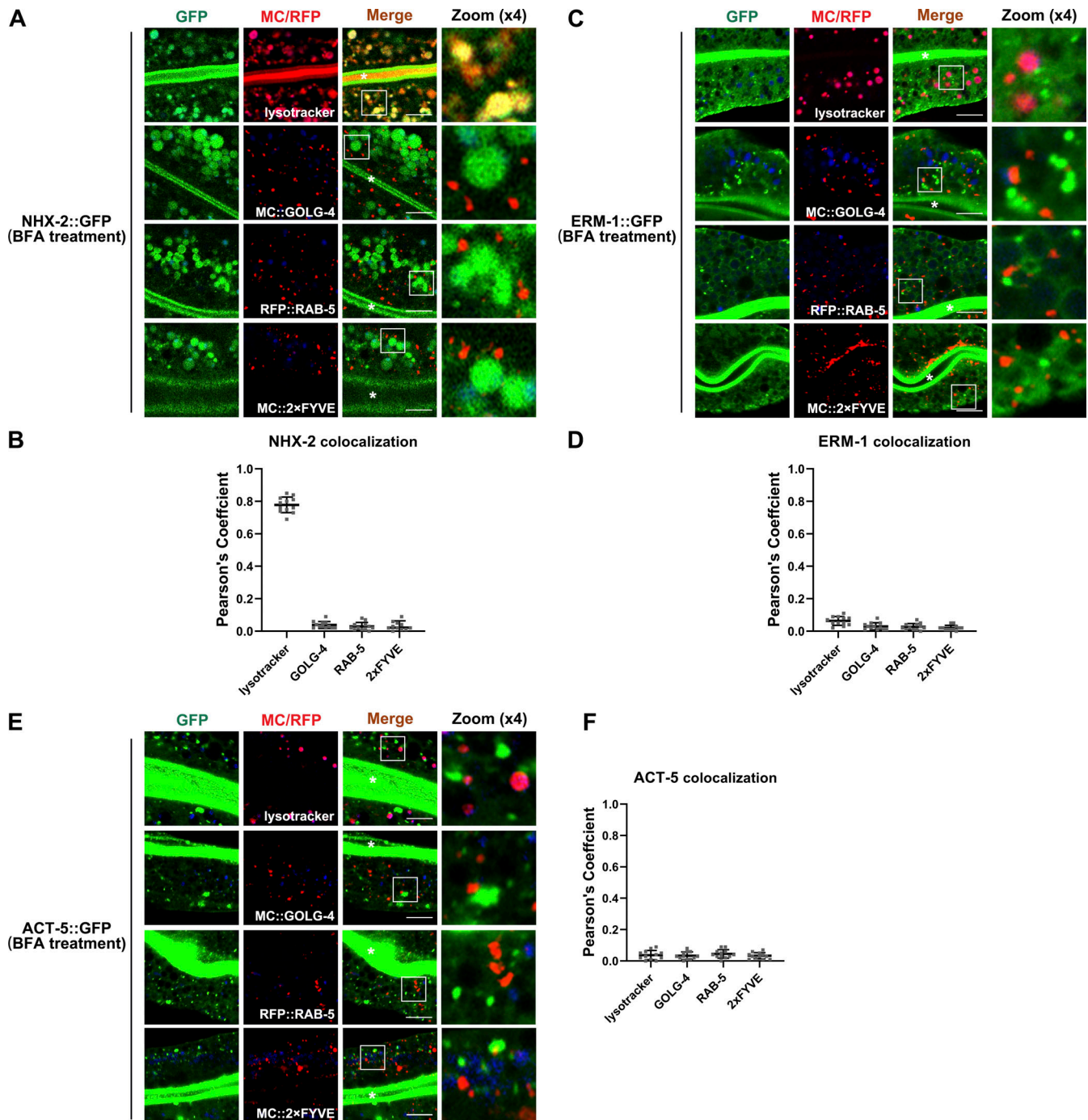


Figure 3. **NHX-2, ERM-1 and ACT-5 accumulate in BFA-treated cells, and part of NHX-2 enters the degradation route.** (A and B) Confocal images showing colocalization between NHX-2::GFP and mCherry/RFP-tagged GOLG-4, RAB-5, 2xFYVE or lysotracker in BFA-treated intestinal cells. Enlarged NHX-2 structures partially overlapped with the lysotracker-labeled lysosome and did not colocalize with GOLG-4, RAB-5 or 2xFYVE. (C and D) Confocal images showing colocalization between ERM-1::GFP and mCherry/RFP-tagged GOLG-4, RAB-5, 2xFYVE or lysotracker in BFA-treated intestinal cells. ERM-1 puncta did not overlap with GOLG-4, RAB-5, 2xFYVE or lysotracker. (E and F) Confocal images showing colocalization between ACT-5::GFP and mCherry/RFP-tagged GOLG-4, RAB-5, 2xFYVE or lysotracker in BFA-treated intestinal cells. ACT-5-labeled structures did not overlap well with GOLG-4, RAB-5, 2xFYVE or lysotracker. Pearson's correlation coefficients for GFP and mCherry signals are calculated ($n = 12$ animals). The signals from the apical membrane were avoided by manual ROI selection. Scale bars: 10 μ m. White asterisks indicate intestinal lumen.

constitutively active RAB-8(Q67L) (Fig. 4, D and E). Importantly, *in vitro* GEF activity assays demonstrated that GST-SMGL-1 facilitated the release of MANT-GDP (2'-/3'-O-[N'-methylanthraniloyl] guanosine-5'-O-diphosphate) from RAB-8

(Fig. 4 F). In contrast, GST-SMGL-1 could not trigger the MANT-GDP release from RAB-5 or GDP-locked (inactive) RAB-8(T22N) (Fig. S2, I and J). We further assessed the regions in SMGL-1 that are implicated in the GEF activity toward RAB-8.

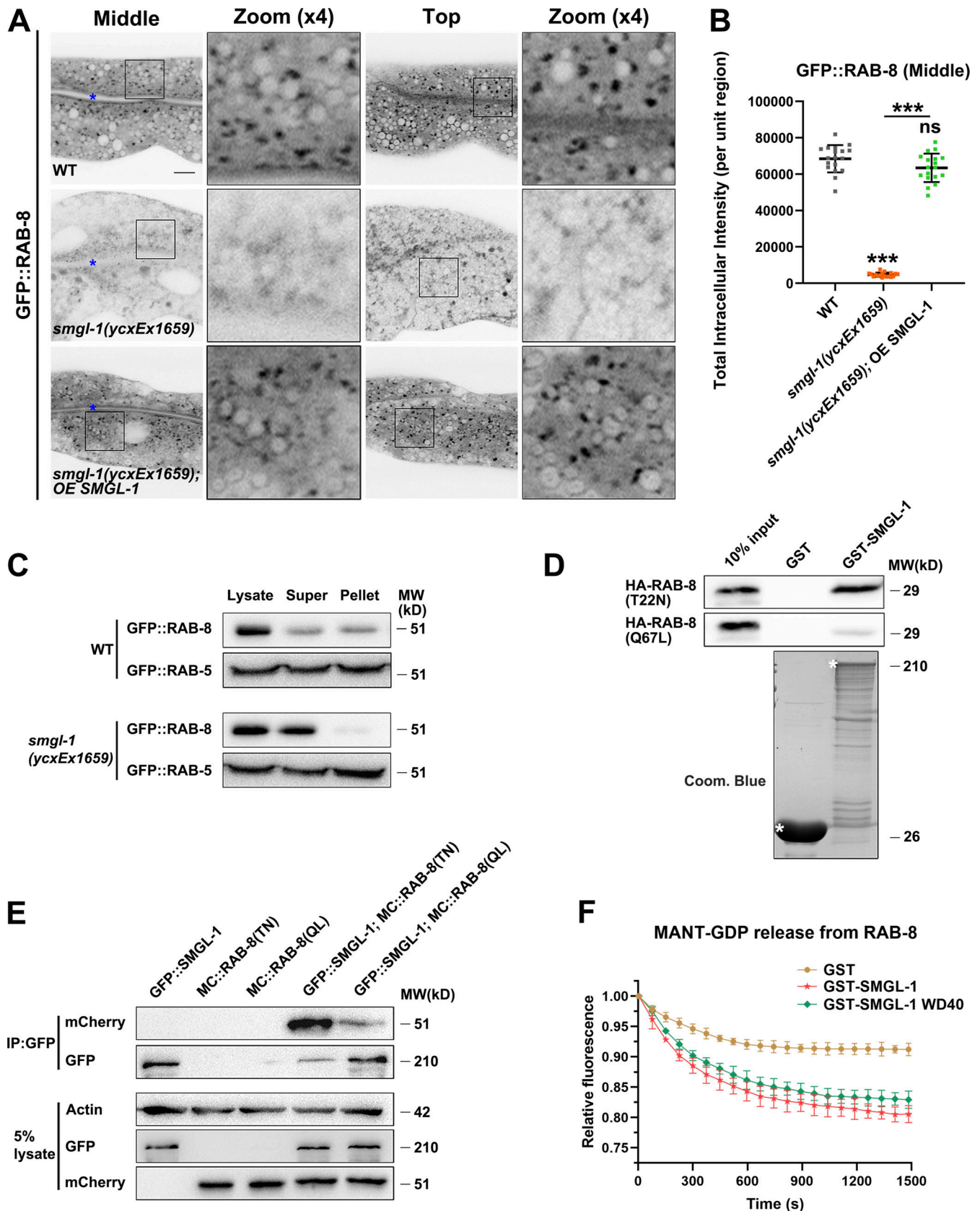


Figure 4. **SMGL-1 functions as a guanine nucleotide exchange factor for RAB-8.** (A and B) Confocal images of intestinal cells expressing GFP-tagged RAB-8. Compared with wild-type animals, *smgl-1* knockout reduced the intensity of GFP::RAB-8-labeled puncta. Overexpression of CRISPR/Cas9-editing resistant SMGL-1 rescued the localization defects of GFP::RAB-8 in *smgl-1* knockout animals. The signals from the apical membrane were avoided by manual

ROI selection. Data are shown as mean \pm SD ($n = 18$ each, six animals of each genotype sampled in three different unit regions of each intestine defined by a 100×100 [pixel²] box positioned at random). For multiple comparisons, statistical significance was determined using a one-way ANOVA followed by a post-hoc test (Dunn's Multiple Comparison Test). ***, $P < 0.001$. Data distribution was assumed to be normal, but this was not formally tested. Scale bars: 10 μ m. Colored asterisks indicate intestinal lumen. **(C)** Western blot showing GFP-tagged RAB-8 and RAB-5 in worm lysate, supernatant, and pellet. The membrane-to-cytosol (pellet-to-supernatant) ratio of RAB-8 decreased in *smgl-1(ycxEx1659)* mutants. In contrast, the ratio of GFP::RAB-5 (early endosome marker) was not affected by SMGL-1 knockout. **(D)** Western blot showing GST pull-down with in vitro translated HA-tagged proteins. GST-SMGL-1 interacted with HA-RAB-8(T22N) while displaying little affinity for HA-RAB-8(Q67L). **(E)** In a co-immunoprecipitation assay, SMGL-1 precipitated predominantly with RAB-8 (T22N) inactive form. **(F)** In vitro GEF assay. MANT-GDP release from RAB-8 was measured by adding GST-only, GST-SMGL-1, and GST-SMGL-1(WD40 domain). GST-SMGL-1 and GST-SMGL-1(WD40 domain) promoted the release of MANT-GDP from RAB-8. However, GST-only failed to trigger the MANT-GDP release from RAB-8. Source data are available for this figure: SourceData F4.

Although the N-terminal WD40 domain possesses GEF activity in vitro (Fig. 4 F), its overexpression failed to rescue the PGP-1 accumulation phenotype in *smgl-1(ycxEx1659)* mutants (Fig. 5, A and B), suggesting that the C-terminus of SMGL-1 is indispensable to the in vivo exercise of GEF efficacy. Previous work has shown that the EHBP-1 preferentially binds to active RAB-8(GTP) (Shi et al., 2010). Our biochemical results confirmed this binding preference and showed that the loss of SMGL-1 led to a \sim 50% reduction in interactions between EHBP-1 and RAB-8 (Fig. S2, K and L), indicating a decrease in RAB-8 activity. Taken together, these results introduced SMGL-1 as a novel GEF, promoting the activation of RAB-8.

Mammalian Rabin8 has been reported to exert GEF activity to drive the activation of Rab8 (Hattula et al., 2002). In *C. elegans*, the homolog of Rabin8 is F54C9.11 (hereafter referred to as RABI-8). Unexpectedly, the intensity and number of GFP::RAB-8-positive structures were augmented in RABI-8-deficient cells (Fig. S2, M–O). Consistently, the P/S ratio of GFP::RAB-8 was increased by \sim 2.4 fold in *rabi-8* mutants compared to that in wild-type animals (Fig. S2 P). Furthermore, compared with wild-type animals, the intensity and P/S ratio of GFP::RAB-8 both decreased in *smgl-1(RNAi);rabi-8(tm2518)* animals (Fig. S2, M, N, and Q), resembling that of *smgl-1* mutants. Together, these findings suggested that in the *C. elegans* intestine, RABI-8 acts to restrain the activity of RAB-8 and SMGL-1 functions as a bona fide GEF toward RAB-8.

Expression of constitutively active RAB-8 variant relieves the unconventional secretion defects caused by SMGL-1 deficiency

Our observation that SMGL-1 acts as a GEF of RAB-8 suggested that RAB-8 activation is an essential event in SMGL-1-mediated apical Type IV UPS. To directly evaluate the requirement for the RAB-8 activity, we examined the effect of the overexpression of constitutively active RAB-8(Q67L) and the inactive RAB-8(T22N) on the apical Type IV UPS. Notably, the ectopic expression of RAB-8(Q67L), but not RAB-8(T22N), alleviated defects in GFP::PGP-1 and PEPT-1::GFP secretion in the *smgl-1(ycxEx1659)* mutant (Fig. 5, A–D). Conversely, the overexpression of early/sorting and late endosome associated RAB-5, RAB-6.2, RAB-7, and RAB-10 did not mitigate the defects in PGP-1 secretion under SMGL-1 knockout (Fig. S3 A). Together, these results indicated that SMGL-1-mediated RAB-8 activation is required for the apical Type IV UPS.

NBAS, the mammalian homolog of SMGL-1, has been reported to participate in the Golgi-to-ER retrograde transport (Aoki et al., 2009). To determine whether the SMGL-1/RAB-8

functional module is involved in this process within the *C. elegans* intestine, we assayed the distribution of retrograde cargo protein RER-1, which encodes a cis-Golgi-located receptor for ER membrane proteins (Sato et al., 2001). GFP::RER-1 was mislocalized to tiny puncta throughout the cytosol of *smgl-1(ycxEx1659)* mutant cells (Fig. 5, E and F), presumably non-tethered vesicles. However, RAB-8 deficiency did not compromise the distribution of GFP::RER-1, and RAB-8(Q67L) overexpression failed to reestablish GFP::RER-1 localization in SMGL-1-depleted cells (Fig. 5, E and F). In addition, the loss of SMGL-1 had no discernible effects on the distribution of AMAN-2-labeled cis-/medial-Golgi or GOLG-4-labeled TGN (Fig. S3, B and C; Munro, 2011; Sato et al., 2011). Together, these observations suggested that the defect in apical PGP-1 or PEPT-1 secretion associated with loss of SMGL-1/RAB-8 module was unlikely due to the inhibition of Golgi-to-ER retrograde transport or impaired integrity of Golgi.

We further probed whether the intracellular accumulation of PGP-1 could be attributed to defects in the retrieval of internalized PGP-1 to the plasma membrane. SMGL-1 deficiency did not compromise the localization of recycling regulators SNX-3, SDPN-1, ARF-6, and RME-1 (Fig. S3, D–G; Gleason et al., 2016; Chen et al., 2018; Lin et al., 2001; Tian et al., 2021). Then, we assayed the localization of PGP-1 in multiple mutants defective in endocytic recycling. The depletion of recycling regulator RAB-10 did not affect the distribution of PGP-1 (Fig. 1, C and D). Likewise, PGP-1 did not accumulate in intracellular structures in animals lacking ARF-6, SDPN-1, and RME-1 (Fig. S3 H), which are all involved in the slow recycling process. SNX-17/Snx17 and SNX-27/Snx27 are sorting nexins implicated in the retrograde transport from endosomes (Steinberg et al., 2012). Neither SNX-17 nor SNX-27 deficiency caused aberrant PGP-1 localization (Fig. S3 H). Furthermore, in *smgl-1* knockdown animals, accumulated PGP-1 showed little colocalization with RAB-5 (early endosome), SDPN-1 (early and recycling endosome), SNX-3 (early and recycling endosome), and RME-1 (recycling endosome; Fig. S3 I). RAB-5 is a key regulator in early endosomes (Sato et al., 2005; Liu et al., 2018), and RAB-35 regulates fast recycling from early endosome to plasma membrane (Sato et al., 2008). Interestingly, we observed a prominent PGP-1 accumulation in RAB-5 and RAB-35 knockdown animals (Fig. S3 H). Taken together, our results were consistent with the notion that the intracellular retention of PGP-1 likely reflects a defect in UPS, and regulatory machinery of fast recycling could also participate in the exocytosis of PGP-1.

Furthermore, we analyzed whether the accumulation of PGP-1 in SMGL-1-depleted cells is due to defects in endocytosis.

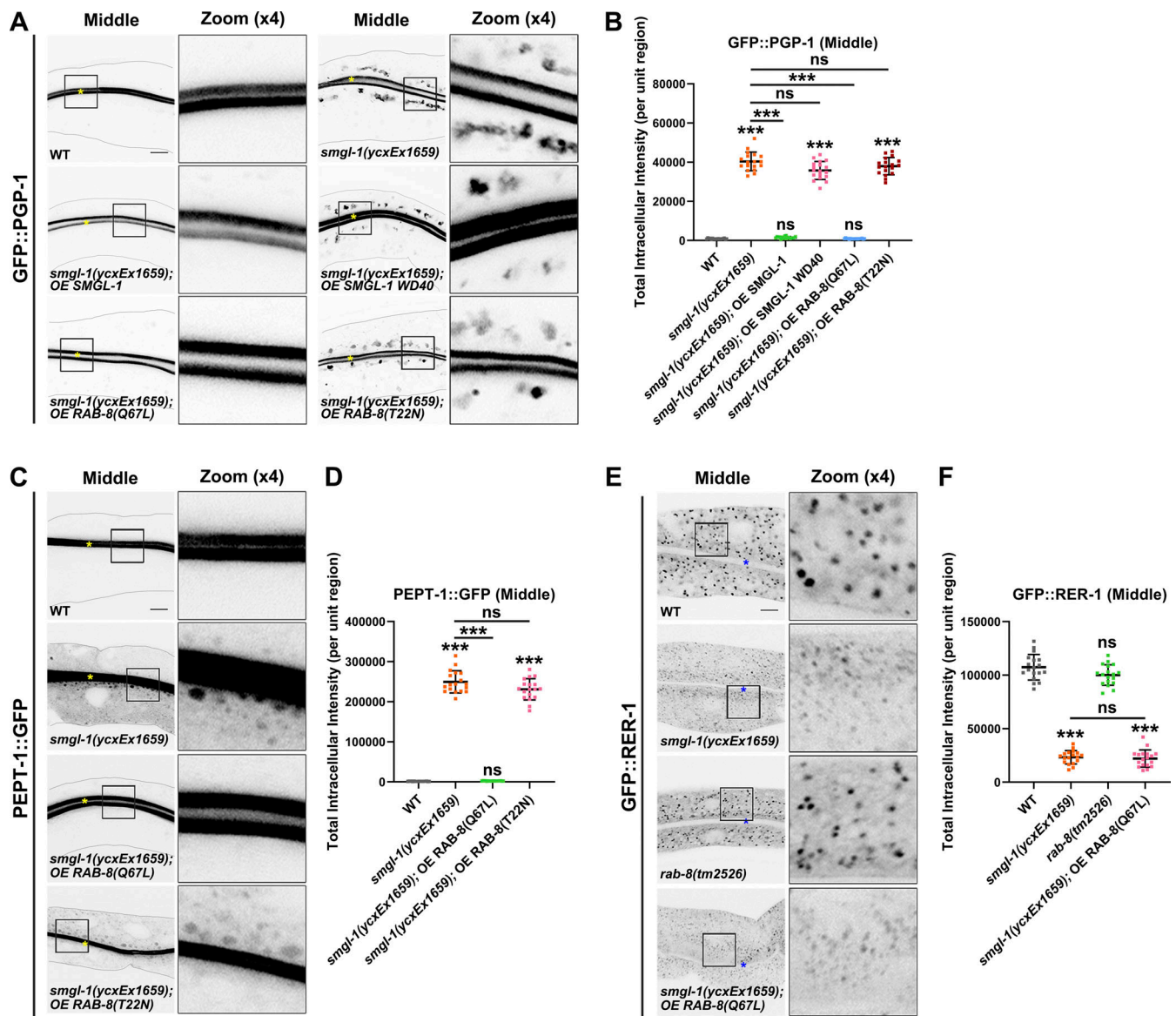


Figure 5. Expression of constitutively active RAB-8 alleviates the secretion defects of PGP-1 and PEPT-1 caused by SMGL-1 deficiency. (A and B) Confocal images of intestinal cells expressing GFP-tagged PGP-1. Compared with wild-type animals, overexpression of the WD40 domain of SMGL-1 failed to rescue the intracellular accumulation phenotypes of GFP::PGP-1 in *smgl-1(ycxEx1659)* mutants. Overexpression of RAB-8(Q67L), but not RAB-8(T22N), restored the intracellular accumulation phenotypes of GFP::PGP-1 in *smgl-1(ycxEx1659)* mutants. **(C and D)** Confocal images of intestinal cells expressing GFP-tagged PEPT-1. Compared with wild-type animals, overexpression of RAB-8(Q67L), but not RAB-8(T22N), restored the intracellular accumulation phenotypes of PEPT-1::GFP in *smgl-1(ycxEx1659)* mutants. **(E and F)** Confocal images of intestinal cells expressing GFP::RER-1. GFP::RER-1 normally resides in the intracellular punctate structures. In *smgl-1(ycxEx1659)* mutants, GFP::RER-1 appeared diffusive and labeled small puncta. Loss of RAB-8 did not affect the localization of GFP::RER-1, and overexpression of RAB-8(Q67L) failed to restore the localization of GFP::RER-1 in *smgl-1* mutants. The signals from the apical membrane were avoided by manual ROI selection. Data are shown as mean \pm SD ($n = 18$ each, six animals of each genotype sampled in three different unit regions of each intestine defined by a 100×100 [pixel²] box positioned at random). For multiple comparisons, statistical significance was determined using a one-way ANOVA followed by a post-hoc test (Dunn's Multiple Comparison Test). ***, $P < 0.001$. Data distribution was assumed to be normal but this was not formally tested. Scale bars: 10 μ m. Colored asterisks indicate intestinal lumen.

Clathrin and AP-2 mediate the internalization of multiple membrane proteins. In *C. elegans*, CHC-1 encodes the clathrin heavy chain. CHC-1 deficiency led to abnormal aggregation of PGP-1 in the apical membrane, which is quite different from the pattern in *smgl-1* mutants (Fig. S3 J). APA-2 and APB-1 constitute *C. elegans* counterparts of the AP-2 α and β subunit, respectively. Knockdown of APA-2 and APB-1 often caused the ring-like

structures of PGP-1 in the periphery of the apical membrane (Fig. S3 J). These subapical ring-like structures were rarely observed in SMGL-1-deficient animals. Myosin VI is reported to regulate the endocytosis of Type IV UPS cargo CFTR (Collaco et al., 2010). Knockdown of HUM-8, the *C. elegans* homolog of Myosin VI, resulted in similar subapical ring-like structures (Fig. S3 J). This series of evidence indicated that endocytic

defects are not likely to underlie intracellular accumulation of PGP-1 in *smgl-1* mutants.

SMGL-1 resides in the ER-Golgi intermediate compartment and adjacent RAB-8-positive endosomal structures

To gain an assessment of the distributional pattern of SMGL-1, we first generated transgenic animals expressing intestine-specific GFP::SMGL-1. Live-cell imaging revealed that GFP::SMGL-1 resides in punctate structures in the intestinal cells of wild-type animals (Fig. S4 A). Furthermore, we generated a knock-in (KI) FLAG-SMGL-1 reporter via the CRISPR/Cas9 system to add an epitope tag (2xFLAG) to the N-terminus of endogenous SMGL-1. Similarly, endogenous SMGL-1 was localized to distinct cytoplasmic puncta (Fig. S4 B). Specifically, expression of both transgenic GFP::SMGL-1 and endogenous SMGL-1 can be largely abolished by RNAi-mediated knockdown or CRISPR/Cas9 knockout (Fig. S4, A–E).

To better appreciate the function of SMGL-1 in apical Type IV UPS, we performed colocalization assays to define the compartments in which SMGL-1 resides. We observed that SMGL-1 overlapped well with the ER-Golgi intermediate compartment (ERGIC) markers ILE-1/ERGIC-53, and the *cis*-Golgi-located retrograde cargo protein RER-1 and ARF-1.2/Arf1 (Fig. 6, A and B; Aoki et al., 2009; Tagaya et al., 2014; Appenzeller-Herzog and Hauri, 2006; D'souza-Schorey and Chavrier, 2006). Unlike vertebrate cells, which contain a juxtannuclear Golgi apparatus, Golgi mini-stacks are scattered throughout the cytoplasm of *C. elegans* intestinal epithelial cells. Notably, we noticed that the GFP::SMGL-1 appeared closer in proximity to AMAN-2-labeled *cis*-/medial-Golgi than to GOLG-4-labeled TGN (Fig. 6, A and B). A similar juxtaposition was observed between ILE-1::GFP and AMAN-2::RFP (Fig. S4, F and G). Prominently, the SMGL-1 fluorescence signal frequently overlapped with that of RAB-8 in punctate structures (Figs. 6, C and D; and S4, H and I) but displayed little overlap with the early endosome marker RAB-5, the lysosome marker LAAT-1, or the basolateral recycling endosome marker RME-1 (Fig. S4, J and K). Concurrent residency of SMGL-1 in ERGIC and RAB-8-labeled structures led us to assume that RAB-8 could also be located in the ERGIC zone. Indeed, we observed a partial colocalization between ILE-1 and RAB-8 (Pearson's coefficient: ~40%; Fig. 6, C and D). Consistently, our co-immunoprecipitation assay showed that RAB-8 could interact with ILE-1 (Fig. 6 E). Of note, a recent investigation in the mammalian cells identified the ERGIC as a regulatory station of UPS (Zhang et al., 2020), thereby consolidating our findings.

NBAS/NAG reportedly functions as a component of the NRZ (NAG-RINT1-ZW10) tethering complex, mediating Golgi-to-ER retrograde transport (Aoki et al., 2009; Schmitt, 2010; Tagaya et al., 2014). No ortholog of RINT1 has been identified in *C. elegans*, while CZW-1 encodes a homolog of ZW10 (Yamamoto et al., 2008). To determine whether the components of the NRZ complex play a role in the localization and affiliated function of SMGL-1 in intestinal cells, a series of assays were performed. First, we found that CZW-1 overlapped well with SMGL-1 and a subset of RAB-8 (Figs. 7, A and B and S5 A), and CZW-1 interacted with SMGL-1 (Figs. 7 C and S5 B). Nevertheless, the presence of GST-CZW-1 had no significant effect on the GEF

activity of GST-SMGL-1 *in vitro* (Fig. S5 C), suggesting that CZW-1 could solely be involved in the subcellular localization of SMGL-1. Indeed, CZW-1 knockdown led to the dispersion of GFP-tagged SMGL-1 and RAB-8 from the punctate structures (Fig. 7, D–G). Moreover, consistent with the requirement of CZW-1 for SMGL-1 residency, overexpression of SMGL-1 restored the punctate labeling of GFP::RAB-8 in *czw-1(RNAi)* animals (Fig. 7, F and G). Likewise, overexpression of SMGL-1 or active RAB-8(Q67L) alleviated the distribution defects of GFP::PGP-1 in CZW-1 knockdown cells (Fig. 7, H and I). To determine whether there is reciprocal regulation between CZW-1 and SMGL-1, we examined the subcellular localization of CZW-1 in *smgl-1* mutants. In this respect, the loss of SMGL-1 did not affect the GFP::CZW-1 distribution (Fig. S5 D), and CZW-1 overexpression failed to reestablish the proper localization of GFP::RAB-8 or GFP::PGP-1 in *smgl-1* mutants (Fig. S5, E and F). Besides, SMGL-1 or RAB-8 overexpression did not restore the localization of Golgi-to-ER retrograde cargo GFP::RER-1 in CZW-1 knockdown animals (Fig. S5 G). Taken together, our results demonstrated a unidirectional regulation between CZW-1 and SMGL-1, with CZW-1 facilitating the subcellular localization of SMGL-1.

The expressions of SMGL-1 and RAB-8 can be affected by infection-related conditions

C. elegans has been set up as a model to study bacterial infection and host response (Mahajan-Miklos et al., 1999; Tan et al., 1999a; Tan et al., 1999b). In this respect, *C. elegans* PGP proteins are closely associated with the resistance to the infection of *P. aeruginosa* strain PA14 (Mahajan-Miklos et al., 1999; Kurz et al., 2007). Since our data indicated that SMGL-1 and RAB-8 regulate the unconventional secretion of PGP-1, we sought to determine whether the expression of the SMGL-1/RAB-8 functional module can respond to *P. aeruginosa* infection. Interestingly, after PA14 treatment for 8 h, GFP::SMGL-1 and GFP::RAB-8 accumulated in the enlarged cytosolic structures, which was likely due to the elevated expression of both proteins (Fig. 8, A–E).

C. elegans p38 MAP kinase pathway was initially identified in a genetic screen for mutants with increased susceptibility to *P. aeruginosa* infection (Kim et al., 2002). Mechanistic dissection revealed that the p38 MAP kinase cascade acts as a major signaling cascade in the intestinal innate immune response (Kim et al., 2002). Given that the infection-boosted expression of SMGL-1 and RAB-8 implicates the apical Type IV UPS as a host defense mechanism in *C. elegans*, it is rational to speculate that the deficiency of innate immunity could also promote the expression of SMGL-1. Supporting this conjecture, the mRNA level of SMGL-1 was elevated upon PMK-1/p38 MAP kinase knockdown (Fig. 8 F). Furthermore, we examined whether there is a mutual impact between the SMGL-1/RAB-8 module and innate immunity by probing the expression of a set of antimicrobial peptides (AMPs) genes that are up-regulated during infection (Pujol et al., 2008a; Pujol et al., 2008b; Engelmann and Pujol, 2010; Dierking et al., 2011). To this end, we observed that the mRNA levels of the neuropeptide-like protein (*nlp*) and caenacin (*cnc*) family genes were all enhanced in SMGL-1-deficient animals (Fig. 8 G), suggestive of the boosted innate immune response. Taken together, these results suggested that infection-related

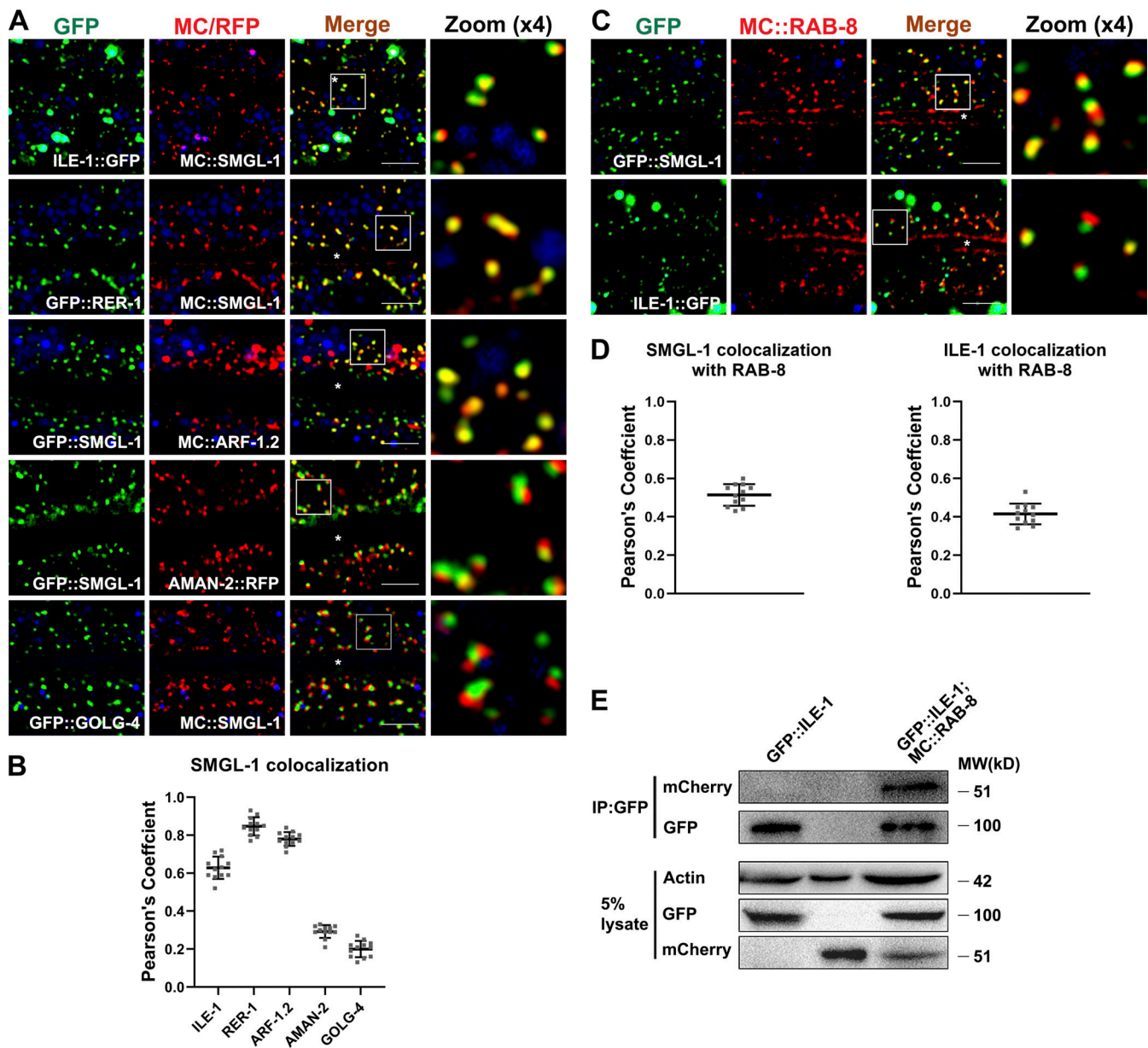


Figure 6. SMGL-1 resides in the ER-Golgi intermediate compartment and adjacent RAB-8-positive structures. (A and B) Confocal images showing colocalization between SMGL-1 and organelle markers in the intestinal cells. SMGL-1 overlapped with the ERGIC marker ILE-1/ERGIC-53 and the *cis*-Golgi-located retrograde cargo RER-1 and ARF-1.2/Arf1. SMGL-1 appeared closer in proximity to AMAN-2-labeled *cis*-/medial-Golgi than to GOLG-4-labeled TGN. **(C and D)** Confocal images showing colocalization between RAB-8 and SMGL-1 or ERGIC marker ILE-1/ERGIC-53 in the intestinal cells. SMGL-1 often overlapped with RAB-8 in punctate structures. Also, RAB-8 partially colocalized with ILE-1. Pearson's correlation coefficients for GFP and mCherry signals were calculated ($n = 12$ animals). The signals from the apical membrane were avoided by manual ROI selection. Scale bars: 10 μ m. White asterisks indicate intestinal lumen. **(E)** In a co-immunoprecipitation assay, ILE-1 precipitated with wild-type RAB-8. Source data are available for this figure: SourceData F6.

conditions can modulate the RAB-8-mediated apical UPS, and there exists an interplay between the SMGL-1/RAB-8 module and innate immune responses.

SMGL-1 and RAB-8 are required for resistance to environmental stressors

Mammalian PGP are broadly expressed in normal and tumor tissues and are critical for drug disposition (Mcgrath and Varshavsky, 1989; Fromm, 2004; Woldemichael et al., 2011; Fu, 2013). Likewise, in addition to being closely associated with

resistance to the infection, *C. elegans* PGPs are implicated in the resistance to environmental stressors (Broeks et al., 1995; Broeks et al., 1996; Mahajan-Miklos et al., 1999). To assess the involvement of the SMGL-1/RAB-8 module in stressors resistance, we scored the survival rate of SMGL-1 knockdown animals in the presence of environmental stressors. Our experiments demonstrated that SMGL-1 deficiency reduced the resistance to colchicine, while RAB-8 overexpression effectively improved the survival rate of SMGL-1 knockdown animals (Fig. 8 H). Then, we examined the heavy metal susceptibility of SMGL-1 knockdown

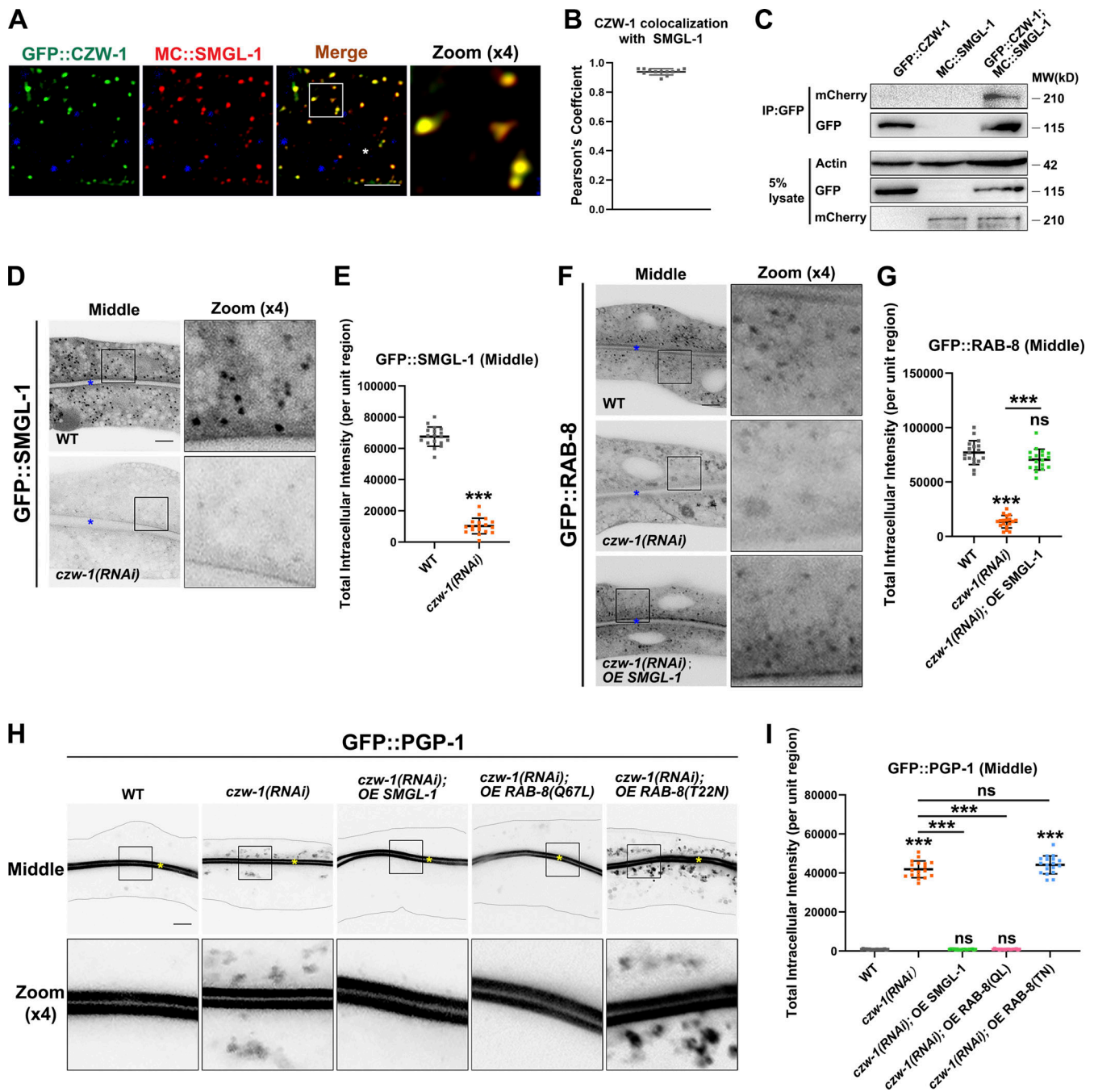


Figure 7. The intracellular localization of SMGL-1 requires CZW-1. (A and B) Confocal images showing colocalization between CZW-1 and SMGL-1 in the intestinal cells. GFP::CZW-1 colocalized extensively with MC::SMGL-1 in punctate structures. Pearson's correlation coefficients for GFP and mCherry signals were calculated ($n = 12$ animals). The signals from the apical membrane were avoided by manual ROI selection. **(C)** In a co-immunoprecipitation assay, SMGL-1 precipitated with CZW-1. **(D and E)** Confocal images of intestinal cells expressing GFP-tagged SMGL-1. The fluorescence intensity of GFP::SMGL-1 puncta was reduced in CZW-1 knockdown cells. **(F and G)** Confocal images of intestinal cells expressing GFP-tagged RAB-8. CZW-1 knockdown reduced the intensity of RAB-8-labeled puncta. Overexpression of SMGL-1 or RAB-8(Q67L) restored the labeling of GFP::RAB-8. **(H and I)** Confocal images of intestinal cells expressing GFP-tagged PGP-1. CZW-1 knockdown led to intracellular accumulation of GFP::PGP-1. Overexpression of SMGL-1 or RAB-8(Q67L) restored the localization defects of GFP::PGP-1. The signals from the apical membrane were avoided by manual ROI selection. Data are shown as mean \pm SD ($n = 18$ each, six animals of each genotype sampled in three different unit regions of each intestine defined by a 100×100 [pixel²] box positioned at random). Statistical significance was determined using a two-tailed, unpaired Student's t test. For multiple comparisons, statistical significance was determined using a one-way ANOVA followed by a post-hoc test (Dunn's Multiple Comparison Test). ***, $P < 0.001$. Data distribution was assumed to be normal but this was not formally tested. Scale bars: 10 μ m. Colored asterisks indicate intestinal lumen. A dotted line indicates the outline of the intestine. Source data are available for this figure: SourceData F7.

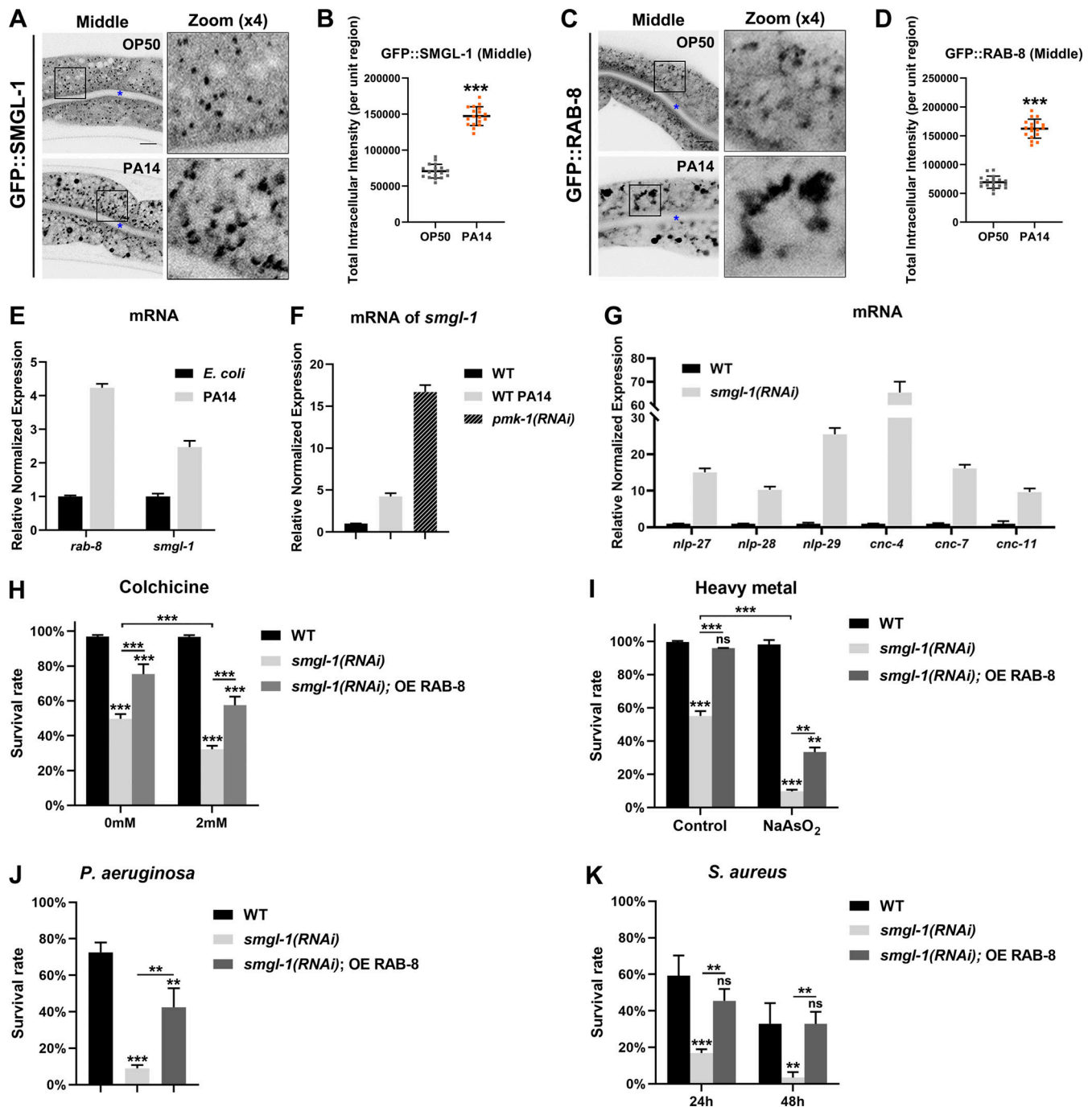


Figure 8. The expressions of SMGL-1 and RAB-8 can be affected by infection-related conditions, and SMGL-1 and RAB-8 are required for resistance to environmental stressors. (A–D) Confocal images of intestinal cells expressing GFP-tagged SMGL-1 and RAB-8. Compared with animals fed on *E. coli* OP50, GFP::SMGL-1 and GFP::RAB-8 accumulated in enlarged structures in the cytosol after PA14 infection. Data are shown as mean \pm SD ($n = 18$ each, six animals of each genotype sampled in three different unit regions of each intestine defined by a 100×100 [pixel²] box positioned at random). Statistical significance was determined using a two-tailed, unpaired Student's *t* test. ***, $P < 0.001$. Data distribution was assumed to be normal, but this was not formally tested. Scale bars: 10 μ m. Colored asterisks indicate intestinal lumen. (E) PA14 treatment increased *smgl-1* and *rab-8* mRNA levels. Each is the average of three replicates. (F) The mRNA level of *smgl-1* increased significantly upon PA14 infection and knockdown of PMK-1. Each is the average of three replicates. (G) The mRNA levels of the neuropeptide-like protein (*nlp*) and caenacin (*cnc*) family genes were all enhanced in SMGL-1 knockdown animals. Each is the average of three replicates. (H) SMGL-1 deficiency reduced the resistance to colchicine, while RAB-8 overexpression improved the survival rate of SMGL-1 knockdown animals. (I) The survival rate was diminished under arsenite exposure, and RAB-8 overexpression promoted survival in animals. (J) After 48 h of *P. aeruginosa* exposure, the survival rate of SMGL-1 knockdown animals was reduced, while RAB-8 overexpression improved the survival rate. (K) SMGL-1 depletion increased susceptibility to *Staphylococcus aureus*, with RAB-8 overexpression improving the survival rate. Data are shown as mean \pm SD. For multiple comparisons, statistical significance was determined using a one-way ANOVA followed by a post-hoc test (Dunn's Multiple Comparison Test). **, $P < 0.01$; ***, $P < 0.001$. Data distribution was assumed to be normal, but this was not formally tested.

animals and found that their survival rate was greatly diminished under arsenite exposure, and RAB-8 overexpression promoted survival in animals (Fig. 8 I). Finally, we validated the significance of SMGL-1 and RAB-8 in defending against environmental bacteria. *Pseudomonas* is a bacterium commonly found in the environment, such as soil and water. When worms were placed onto the lawn of *P. aeruginosa*, the animals would die within 2–3 d (Mahajan-Miklos et al., 1999). After 48 h of exposure, the survival rate of SMGL-1 knockdown animals was reduced to ~10%, while RAB-8 overexpression improved the survival rate to ~40% (Fig. 8 J). Similarly, SMGL-1 depletion increased susceptibility to another environmental pathogen, *Staphylococcus aureus*, with RAB-8 overexpression improving the survival rate (Fig. 8 K). Taken together, these experimental data indicated that the impaired resistance to environmental stressors in SMGL-1 knockdown animals is at least partly due to impaired RAB-8 activation. SMGL-1-RAB-8-facilitated UPS serves as a distinct defense mechanism in *C. elegans*, possibly promoting PGPs on fast tracks to the apical surface facing the digestive lumen.

Discussion

In this study, we revealed the noteworthy roles of SMGL-1 and RAB-8 in the Type IV UPS pathway in *C. elegans* intestinal cells (Fig. 9). SMGL-1 resides in ERGIC and nearby endosomal compartments and functions as a GEF toward RAB-8, promoting UPS of a subset of apical integral proteins under steady-state conditions. Loss of SMGL-1 and RAB-8 makes animals more susceptible to environmental stressors. Furthermore, this SMGL-1-RAB-8 module can efficiently respond to infection-related conditions. Taken together, we established the *C. elegans* intestine as an *in vivo* multicellular model and provided mechanistic insights into RAB-8-dependent UPS.

UPS pathways are conserved across species, mostly non-constitutive (Giuliani et al., 2011; Rabouille et al., 2012; Malhotra, 2013; Rabouille, 2017; Kim et al., 2018; Gee et al., 2018; Dimou and Nickel, 2018). For instance, the Type IV UPS of CFTR or pendrin was induced by the blockade of ER-to-Golgi transport or ER stress (Gee et al., 2011; Jung et al., 2016). In these studies, cells were either transfected with dominant-negative mutants of Sar1-T39N and Arf1-Q71L, which are key components regulating ER-to-Golgi trafficking, or treated with ER stress-inducing drugs, such as ER Ca²⁺-ATPase inhibitor thapsigargin (TG). These strategies are necessary to dissect the mechanism by which CFTR and pendrin bypass Golgi. However, the UPS regulation appears not so straightforward. Depletion of Sec16A, which is critical for COP II vesicle formation and supposed to block ER-to-Golgi transport, inhibited the UPS of CFTR induced by Arf1-Q71L (Piao et al., 2017). Using multicellular *C. elegans* as an *in vivo* system, we proposed that the Type IV UPS pathway exists under physiological conditions, and SEC-16/Sec16 is required for this process (Fig. 2 H). Supporting the presence of the steady-state UPS, Golgi reassembly stacking proteins (GRASPs) facilitate the Golgi-bypass secretion of CFTR without inducing ER stress (Gee et al., 2011). Also, fibroblast growth factor 2 (FGF2) and HIV TAT are constitutively secreted via UPS (Steringer et al., 2015; La Venuta et al., 2015; Debaisieux et al., 2012; Zeitler et al., 2015). Given the diversity and heterogeneity

of UPS pathways, further studies under various cellular or environmental conditions are required to dissect the association between ER stress and Type IV UPS.

RabGAPs primarily harbor conserved TBC (named after Tre-2, BUB2p, Cdc16p) domain. In contrast, there exists a diverse group of structurally unrelated RabGEFs, including Sec2 proteins, DENN proteins, monomer and homodimer VPS9 proteins, multi-subunit TRAPPs (transport protein particles), and heterodimer GEFs (Bos et al., 2007; Muller and Goody, 2018; Barr and Lambright, 2010). Notably, REI-1/SH3BP5, recently identified as RAB-11 GEF in *C. elegans* embryos, does not present any previously characterized GEF domains, further demonstrating the diversity of RabGEFs and their catalytic mechanisms (Sakaguchi et al., 2015; Jenkins et al., 2018). SMGL-1 harbors N-terminal WD40 repeats and the C-terminus full of short α -helices. In the SMGL-1 structure predicted by AlphaFold (Jumper et al., 2021; Varadi et al., 2022), the WD40 repeats present a β -sheet geometric core, which is half-wrapped by multiple short α -helices and exposes accessible interactive surfaces. It has been known that WD repeats could induce oligomerization and form a β -propeller architecture, which is usually composed of seven blades and functions as a protein interaction interface (Schapira et al., 2017). Hence, we speculated that the SMGL-1 could localize to the membrane in the form of oligomers, where it interacts with RAB-8(GDP). Nevertheless, the limited information above is not sufficient to help interpret the GEF activity of SMGL-1. Future structural investigation of SMGL-1 will be required to provide fundamental insights into the functional details of SMGL-1 and the stoichiometry of SMGL-1 and RAB-8.

Our results indicated that PGP-1/ABCB1 is secreted via ERGIC-mediated Golgi-bypassing Type IV UPS in *C. elegans* intestinal epithelia. In nematodes, the protective function of PGPs/P-glycoproteins against environmental stressors, such as natural toxins, heavy metals, and pathogens, has been proposed (Broeks et al., 1995; Broeks et al., 1996; Mahajan-Miklos et al., 1999). Consistently, mammalian PGPs have been suggested to exclude amphipathic drugs from the cell and confer drug resistance of tumor cells by exporting chemotherapeutic drugs (Mcgrath and Varshavsky, 1989; Fromm, 2004; Woldemichael et al., 2011; Fu, 2013). Experiments in mammal cells have shown that P-glycoprotein/ABCB1 is located at various subcellular sites, including plasma membrane and endosome (Fu, 2013), and is presumed to be exocytosed via Golgi apparatus (Molinari et al., 1994; Ameen et al., 2007; Tanaka et al., 2008). However, we cannot rule out the possibility that mammalian cells preferentially exocytose PGPs via UPS under stress conditions, which would lead to the blockage of conventional secretion, just as in the case of the UPS of mutant CFTR/ABCC7 (Gee et al., 2011). Of note, *C. elegans* PGP proteins exhibit 13–16% identity with human CFTR. Here, we showed that the deficiency of SMGL-1/RAB-8-mediated Type IV UPS increased animals' susceptibility to colchicine, arsenite, and pathogenic bacteria, which are likely to be substrates of PGPs.

As a soil-dwelling nematode, *C. elegans* is exposed to natural toxins, pathogenic bacteria, and heavy metals. However, *C. elegans* does not have specialized immune cells, except for the six scavenger-like coelomocytes with limited functions. Since the initial description of *C. elegans* as a model for bacterial infection (Mahajan-Miklos et al., 1999; Tan et al., 1999a; Tan et al., 1999b),

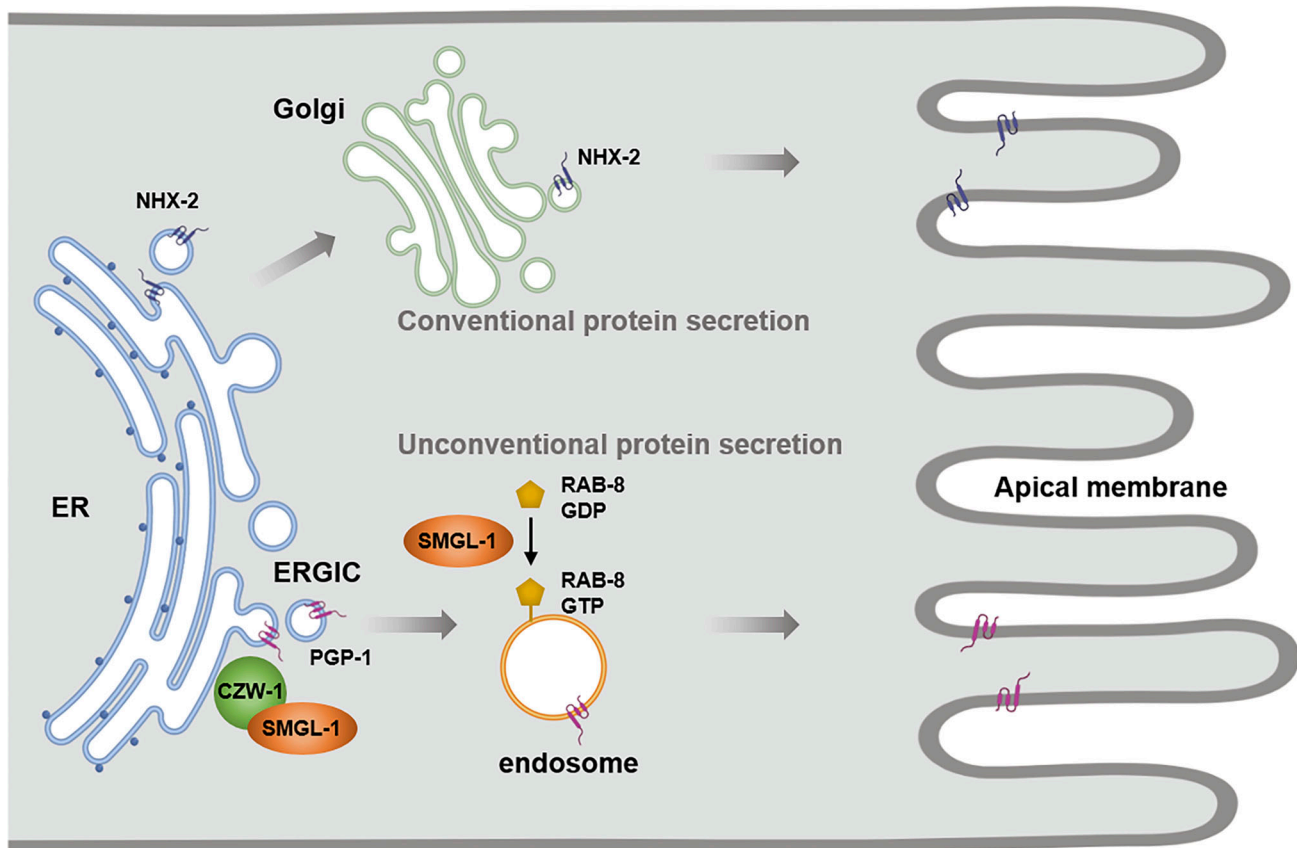


Figure 9. **Model of SMGL-1/RAB-8 regulated apical Type IV UPS.** ERGIC-localized SMGL-1 functions as a GEF towards RAB-8, activating a subset of RAB-8 on nearby endosomal compartments. Apical proteins like PGP-1 are not transported from ER to Golgi. Instead, these cargoes are delivered to RAB-8/SMGL-1 positive endosomes before final delivery to the apical surface.

much progress has been made in identifying key components that mediate the host response in intestinal and epidermal epithelia (Irazoqui et al., 2010; Engelmann and Pujol, 2010). The intestine of *C. elegans* comprises 20 polarized epithelial cells that are non-renewable and share morphological and physiological features with mammalian counterparts. In response to environmental stresses, intestine cells are subjected to the continuous renewal of the plasma membrane, especially on the apical side facing the digestive lumen. Of note, *C. elegans* intestinal cells have been demonstrated as a powerful system for studying membrane trafficking in the context of epithelia in vivo (Chen et al., 2006; Winter et al., 2012; Sato et al., 2014b; Liu et al., 2018). In this study, we established a *C. elegans* multicellular intestine in vivo model to study the Type IV UPS. We propose that the proper operation of Type IV UPS protects worms from environmental stressors, likely by promoting PGPs on fast tracks to the apical surface of intestinal cells. Moreover, our data reveal a potential functional correlation between RAB-8-mediated apical Type IV UPS and innate immunity in the intestinal epithelia.

Materials and methods

General methods and strains

All strains of *C. elegans* were derived from Bristol strain N2. The animals were cultured and maintained according to standard procedures unless indicated otherwise (Brenner, 1974).

RNAi treatment

RNAi-mediated interference was performed according to standard protocols (Timmons and Fire, 1998). The feeding constructs were from the Ahringer library or prepared by PCR from cDNA fragments and cloned into the RNAi vector L4440 (Timmons and Fire, 1998). For most experiments, 4–5 L4 larvae were plated onto the NGM plates containing 1 mM IPTG seeded with dsRNA bacterial clone. The F1 progeny was then examined. For essential genes such as *sar-1*, *rab-1*, and *rab-5*, L1 larvae were plated onto the NGM plates, and young adults were examined. SMGL-1 deficiency has been reported to cause embryonic lethality or sterility (Longman et al., 2007). Hence, in the preliminary stage of this study, an analysis of the *smgl-1(RNAi)* phenotype was performed. When feeding wild-type L1 larvae with *smgl-1(RNAi)* bacteria, there is no significant difference in the animal development of the current generation, including survival rate and growth rate. When feeding wild-type L4 larvae with *smgl-1(RNAi)* bacteria, the hatch rate of F1 (the number of hatched L1 larvae is divided by the number of laid eggs) showed no difference, suggesting that *smgl-1(RNAi)* did not cause embryonic lethality in the F1 generation. Instead, SMGL-1 knockdown mainly induced larval arrest in the F1 generation. To ensure that a certain number of F1 L4 larvae and young adults could be obtained for SMGL-1 deficiency phenotypic analysis, the P0 young adults were inoculated. Moreover, the number of

inoculated animals was deliberately increased to ensure a certain number of F1 adults could be obtained for assays.

Genome-wide RNAi screen

To identify candidate proteins that regulate RAB-8/Rab8, a genome-wide RNAi screen (19,763 genes) was performed in a *rab-10(ok1494)* mutant background using the Ahringer library (Kamath and Ahringer, 2003). The synthetic sterility induced by the simultaneous loss of RAB-10 and candidate proteins were scored. RNAi vector L4440 was used as a negative control, and *rab-8(RNAi)* was deployed as a positive control to validate the soundness of the experimental system. Based on the GO (Gene Ontology) descriptions in WormBase (version: WS283), the single knockdown of numerous genes will produce either embryonic lethality or larval arrest. To cover the whole genome as much as possible, the following strategies were adopted. (1) Inoculated 3–5 parental generation (P0) young adults per well and recorded the number of young adults of F1 generation after 3 d. (2) For each gene, three RNAi replicates were executed, and an N2 wild-type control was used for each replicate. If the number of Filial 1 (F1) young adults yielded by the P0 *rab-10(ok1494)*, young adults were significantly less than that of P0 wild-type animals (the sum of the three groups was subjected to a *t* test), this gene was considered as a positive hit. (3) Those genes whose knockdown caused P0 wild-type young adults (3–5 animals) to produce no or very few (sum of three groups) F1 young adults 3 d later (embryonic lethality or sterility) were excluded.

Heat-shock-inducible CRISPR/Cas9 mutant strains

CRISPR/Cas9 plasmids were prepared according to previously described protocols (Shen et al., 2014; Li et al., 2015). The heat-shock promoter *Phsp-16.2* was used to substitute the *eft-3* promoter in pDD162 (Addgene). CRISPR design tool (<http://crispr.mit.edu>) was used to select the RNA target locations. The three *smgl-1* target sequences were 5'-AATGAGCTATGCCCGTCAACTGG-3', 5'-ATTCCCTCATGCAGTTCTAGAGG-3', and 5'-GATGTA AATTCCGGCTATTTGTGG-3'. CRISPR/Cas9 plasmids transgenic animals were generated by the microinjection of plasmids at 50 ng/μl with a selective marker *Podr-1::gfp* into the N2 hermaphrodites germline.

CRISPR/Cas9 knock-in strains

To generate the 2xFLAG::SMGL-1 and the 2xFLAG::RAB-8 knock-in alleles, donor cocktails were used as repair templates, which can be synthesized using two re-annealed fragments: one was FLAG sequence with 40 bp upstream and downstream homology arms of the guide cut site, and the other was FLAG sequence only, without any homology arms. A single gRNA (sgRNA) template containing T7 promoter (5'-AAGCTAATACGA CTCACTATAGG-3'), sgRNA sequence (*smgl-1* sgRNA: 5'-ACA GAATGGCGCATATGAG-3'; *rab-8* sgRNA: 5'-CGATGTTTTCTT GACATCT-3'), and a trans-activating CRISPR RNA sequence (5'-GTTTTAGAGCTAGAAATAGCAAGTTAAAATAAGGCTAGTCCG TTATCAACTTGAAAAAGTGGCACCGAGTCGGTGTCTTTT-3') were prepared using PCR. The PCR products were used as the template for sgRNA transcription using the HiScribe Quick T7 High Yield RNA Synthesis Kit (E2050; New England Biolabs).

sgRNAs were purified using a Monarch RNA Cleanup Kit (T2040; New England Biolabs). sgRNA and 0.5 μl Cas9 nuclease (10 μg/μl; Integrated DNA Technologies) were incubated at 37°C for 10 min, then repaired using a template donor cocktail (final 40 ng/μl), after which the selection marker pRF4[*rol-6(su1006)*] vectors (final 50 ng/μl) were added. Transgenic strains were obtained using standard microinjection techniques. The candidate F1 animals were identified by following a roller phenotype. The homozygote F2 progenies were identified by PCR and sequencing.

Reporter construction

All vectors were constructed using Gateway technology (Invitrogen). The cDNAs encoding SMGL-1, CZW-1, PGP-1, PEPT-1, SID-2, NHX-2, SLCF-1, ERM-1, ILE-1, GOLG-4, RER-1, SNX-3, APG-1, and CNX-1 were cloned into the entry vector pDONR221 via BP reaction and then transferred into intestinal expression vectors by LR reaction to generate fusion plasmids (Chen et al., 2006). The previously described *vha-6* promoter-driven vectors with a Gateway cassette inserted upstream or downstream of the GFP, mCherry, or FLAG coding region were used (Liu et al., 2018). Plasmids were co-injected with the selective marker *Podr-1::gfp* or *Podr-1::rfp* into the N2 hermaphrodites' germline. At least two stable transgenic lines were analyzed for each reporter.

RNA isolation and quantitative real-time PCR

Young adults were collected using M9 buffer (20 mM KH₂PO₄, 40 mM Na₂HPO₄, 100 mM NaCl, 1 mM MgSO₄). Total RNA was extracted using an RNeasy Plus Mini Kit (QIAGEN) and reverse-transcribed using a Revert Aid RT Kit (Thermo Fisher Scientific). Quantitative PCR reactions were performed using iTaq Universal SYBR Green (Bio-Rad) and a CFX Connect Real-Time PCR Detection System (Bio-Rad). Actin was used as the internal control. The mRNA level in mutant animals was normalized to the level observed in wild-type worms, which was set to one. Error bars indicate the SD of three independent experiments.

In vitro pull-down assay

cDNAs encoding RAB-8(T22N), RAB-8(Q67L) and CZW-1 were cloned into a modified vector pcDNA3.1(+) (Invitrogen) for 2xHA tagging. cDNAs encoding SMGL-1 and CZW-1 were cloned into a pGEX-2T vector (GE Healthcare) for GST tagging. The N-terminally HA-tagged proteins were synthesized in vitro using the TNT-coupled transcription-translation system (Promega). GST fusion proteins were expressed in the ArcticExpress strain of *E. coli* (Stratagene). Bacterial pellets were lysed in 50 ml lysis buffer (50 mM Hepes [pH 7.5], 400 mM NaCl, 1 mM DTT, and 1 mM PMSF) with Complete Protease Inhibitor Mixture Tablets (Sigma-Aldrich). Extracts were cleared by centrifugation, and supernatants were incubated with glutathione sepharose 4B beads (GE Healthcare Life Sciences) at 4°C for 6 h. Beads were washed six times with cold STET buffer (10 mM Tris-HCl [pH 8.0], 300 mM NaCl, 1 mM EDTA, and 0.1% Tween-20). In vitro synthesized HA-tagged proteins were incubated with Glutathione Sepharose 4B beads. After six washes with STET buffer, the eluted proteins were separated on

SDS-polyacrylamide-gel electrophoresis and blotted to nitrocellulose. After blocking and washing with TBST buffer (20 mM Tris [pH 7.5], 150 mM NaCl, 0.1% Tween-20), the blot was probed with an anti-HA antibody.

Co-immunoprecipitation assay

Adult animals were collected with M9 buffer (9 cm plates × 10). About 100 µl worm pellet resuspended in ice-cold lysis buffer (25 mM Tris-HCl [pH 7.5], 100 mM NaCl, 1 mM EDTA, 0.5% NP-40, 1 mM PMSF, 1 mM DTT, 1 mM Na₃VO₄, and 10 mM NaF) containing protease inhibitor cocktail (Sigma-Aldrich). Then, the worm pellet was lysed with an automatic grinding machine (Jingxin Inc.) at 65 Hz for 5 min (10 s interval after every minute). The lysates were centrifuged at 12,000 *g* for 10 min at 4°C. The supernatant was collected and incubated with GFP-Trap Agarose (Chromotek) for 2 h at 4°C. Precipitates were washed 5 × 10 min with lysis buffer and subjected to immunoblotting with anti-mCherry, anti-GFP, and anti-actin antibodies.

Membrane fractionation assay

Wild-type and mutant animals expressing intestinal GFP fusion proteins were synchronized and collected as young adults (9 cm plates × 10). Animals were washed off with M9 buffer, and the pellet was resuspended in 500 µl lysis buffer (50 mM Tris-HCl [pH 8.0], 20% sucrose, 10% glycerol, 1 mM DTT, and protease inhibitor). The worms were lysed and centrifuged at 1,000 *g* for 10 min at 4°C. About 200 µl of the cleared lysate was centrifuged at 100,000 *g* for 1 h. Supernatants were collected, and pellets were reconstituted in the same volume of lysis buffer. Equal volumes of supernatants and pellets were subjected to immunoblotting with anti-GFP and anti-actin antibodies.

In vitro GEF assay

MANT is a fluorescent analog with Ex/Em = 355/448 nm, which can be used to label nucleotides. The compact nature of the MANT fluorophore would lead to minimal perturbation of nucleotide-protein interactions (Pai et al., 1990). In this study, 50 µM MANT-GDP (Invitrogen) was incubated with 500 pmol 6xHis-RAB-5 or 6xHis-RAB-8 (the AKTA system equipped with Superdex 200 or Superose 6 size exclusion chromatography was utilized to improve proteins purification quality) in the pre-loading buffer (50 mM Tris-HCl [pH 8.0], 110 mM NaCl, 1 mM EDTA, 0.8 mM DTT, and 0.005% Triton X-100). After Rab pre-loading at 25°C for 60 min, 10 mM MgCl₂ was added to stop the reaction. Then, 200 pmol preloaded RAB-5 or RAB-8 was incubated with 100 pmol GST-tagged proteins in a GEF buffer (50 mM Tris [pH 8.0], 150 mM NaCl, and 0.5 mM MgCl₂) at 25°C for 100 s. The nucleotide exchange reaction (the dissociation of MANT-GDP from Rab proteins) was triggered by adding the hydrolysis-resistant GTP analog GMP-PNP (Merck) at a final concentration of 0.1 mM. Since the fluorescence emitted by MANT nucleotides decreases upon its dissociation from Rabs, the reduced fluorescence of MANT-GDP can be used to monitor GEF activity. The nucleotide exchange reaction was recorded using a Synergy 2 Multi-Mode Reader (BioTek) at an excitation wavelength of 366 nm and an emission wavelength of 443 nm (Sakaguchi et al., 2015).

BFA and AG1478 microinjection

About 5 µM BFA (Beyotime) or 14 µM AG1478 (Selleckchem) diluted in 0.2% DMSO were microinjected into day-1 adult intestines. Worms were allowed to recover at 20°C for 2 h before examination.

Deglycosylation assay

PNGase F and Endo H treatments were conducted following the manufacturer's instructions (New England Biolabs). Day-1 adult animals expressing FLAG::PGP-1, FLAG::SID-2, and GFP::CNX-1 were lysed. The lysates were centrifuged at 12,000 *g* for 10 min at 4°C. The supernatant was collected and incubated with Anti-FLAG Affinity Gel (Beyotime) or GFP-Trap Agarose (Chromotek) for 2 h at 4°C. Proteins were denatured with Glycoprotein Denaturing Buffer at 100°C for 10 min. About 10 µg proteins were mixed with 2 µl enzyme, 2 µl GlycoBuffer 2 (for PNGase F) or GlycoBuffer 3 (for Endo H), and H₂O to make a 20 µl total volume. The mixtures were incubated at 37°C for 2 h. The proteins were resolved by SDS-PAGE and probed by an anti-FLAG or anti-GFP antibody.

Immunofluorescence staining

Isolated intestines were fixed in 4% paraformaldehyde for 15 min, permeabilized in phosphate-buffered saline (PBS) with 0.5% Triton X-100 for 20 min, blocked in PBS with 1% bovine serum albumin for 30 min, and incubated with anti-FLAG antibodies (1:200; Sigma-Aldrich) at 4°C for 2 h. The intestines were washed three times and incubated with rhodamine-conjugated or FITC-conjugated secondary antibodies.

LysoTracker staining

Adult animals were soaked in 80 µl M9 buffer containing 5 µM LysoTracker Red DND 99 (Invitrogen). Staining was performed for 1.5 h at 20°C in the dark. Worms were then transferred to NGM plates with fresh OP50 and allowed to recover at 20°C for 2 h in the dark before microscopy.

Bacterial resistance assay

PA14 culture was grown at 25°C overnight and spread on NGM plates. *Staphylococcus aureus* was grown at 37°C overnight and spread on LB medium, including 2 mg/ml tryptophan. After spreading the bacterial culture, plates were incubated at 37°C for 24 h and then placed at room temperature for 8–12 h. Twenty L4 larvae treated with control RNAi or *smgl-1* RNAi on NGM plates were transferred to these assay plates and incubated at 25°C. Mortality was scored after 24 and 48 h. Animals were considered dead if they failed to respond to a gentle tap on the head and tail with a platinum wire. The *E. coli* strain OP50 was used as a control for the assays. Three independent assays were performed for each experiment.

Drug sensitivity assay

15 young adult hermaphrodites were plated onto the NGM plates containing 2 mM colchicine (TargetMol) and allowed to lay eggs for 24 h. The parents were then removed, and the eggs were counted. The survival rate was calculated as the total number of adults divided by the number of eggs. Three independent assays were performed for each experiment.

Heavy metal exposure assay

Young adult hermaphrodites were plated onto the NGM plates containing NaAsO₂ (2 mM, Sigma-Aldrich) for 24 h to lay eggs. About 20 L1 larvae (F1) were transferred back to regular NGM plates. Survival rate was calculated as the total number of animals that resumed development divided by 20, the initial number of larvae. Three independent assays were tested for each experiment.

Microscopy and imaging analysis

Fluorescence images (GFP, mCherry, and DAPI channels) were obtained at 20°C using a C2 laser scanning confocal microscope (Nikon) equipped with a 100× NA 1.2 oil-immersion objective and captured using NIS-Elements AR 4.40.00 software. The Z-series of the optical sections were acquired using a 0.8-μm step size. Fluorescence data from the GFP channel were analyzed using Metamorph software version 7.8.0.0 (Universal Imaging). The “Integrated Morphometry Analysis” function of Metamorph was used to measure the fluorescent intensity (total intracellular intensity, a composite index of endosomal quantity and mean intensity) and the fluorescent area within unit regions. From a total of six animals of each genotype, “total intracellular intensity” and “total area” were sampled in three different unit regions of each animal defined by a 100 × 100 (pixel²) box positioned at random ($n = 18$ each). Signals from the apical membrane were avoided when using Metamorph for manual ROI selection. Colocalization images were quantified using Fiji (Image J) software. Pearson’s correlation coefficients for GFP and mCherry signals were calculated, and the entire imaging area of 12 animals was analyzed for most samples. PGP-1 has high labeling densities in the apical membrane, which could artificially inflate Pearson’s measurements. Therefore, signals from the apical membrane were deliberately avoided when using Metamorph for manual ROI selection.

Statistical analysis

The significance of differences and 95% confidence intervals were assessed and plotted using Prism software version 8.02 (GraphPad Software). SD was used as the y-axis error bars for bar charts plotted from the mean values. Two-tailed unpaired Student’s *t* test and one-way ANOVA followed by a post-hoc test (Dunn’s Multiple Comparison Test) were performed.

Online supplemental material

Fig. S1 shows the distribution of apical proteins (PGP-1, PEPT-1, and SID-2) and basolateral protein (NPY) in SMGL-1- or RAB-8-deficient cells. Also shown are the distributions of AMAN-2, NHX-2, ERM-1, ACT-5, and SLCF-1 in cells lacking SMGL-1 or RAB-8 or cells treated with BFA or AG1478. **Fig. S2** shows the interaction between SMGL-1 and RAB-8. Also shown are in vitro SMGL-1 GEF activity assays of RAB-5 and RAB-8(T22N). **Fig. S3** shows the distribution of PGP-1 in cells lacking other Rabs or endocytosis regulators. Also shown are the unaffected Golgi integrity or recycling regulators distribution in cells lacking SMGL-1. **Fig. S4** shows the residency of SMGL-1 in the ER-Golgi intermediate compartment and adjacent RAB-8-positive structures. **Fig. S5** shows the interaction between CZW-1 and SMGL-1

and in vitro SMGL-1 and CZW-1 GEF activity assays of RAB-8. Also shown are the subcellular localization of CZW-1, RAB-8, PGP-1, and RER-1 in indicated genetic backgrounds. Table S1 is a key resources table contains the information of antibodies, bacterial stains, commercial assays, *C. elegans* strains, recombinant DNA, and software. Table S2 is a primers file that lists the sequences of all primers/oligos.

Acknowledgments

This work was supported by the National Key R&D Program of China (2021YFA1300302), the National Natural Science Foundation of China (32130027), the National Science Fund for Distinguished Young Scholars (31825017), and the Major Research Plan of the Natural Science Foundation of China (91954001) to A. Shi, the National Natural Science Foundation of China (32070703) and the Major Research Plan of the Natural Science Foundation of China (91954113) to L. Lin.

The authors declare no competing financial interests.

Author contributions: Conceptualization: X. Wang, L. Lin, A. Shi. Data curation: X. Wang, L. Lin, A. Shi. Formal analysis: X. Wang, L. Lin, A. Shi. Funding acquisition: L. Lin, A. Shi. Investigation: X. Wang, X. Li, J. Wang, J. Wang, C. Hu, J. Zeng. Methodology: X. Wang, X. Li, L. Lin, A. Shi. Project administration: L. Lin, A. Shi. Resources: X. Wang, X. Li, J. Wang, J. Wang, C. Hu, J. Zeng, L. Lin, A. Shi. Software: X. Wang, L. Lin, A. Shi. Supervision: L. Lin, A. Shi. Validation: X. Wang, L. Lin, A. Shi. Visualization: X. Wang, L. Lin. Writing—original draft: X. Wang, L. Lin, A. Shi. Writing—review & editing: L. Lin, A. Shi.

Submitted: 25 November 2021

Revised: 13 April 2022

Accepted: 4 May 2022

References

- Ameen, N., M. Silvis, and N.A. Bradbury. 2007. Endocytic trafficking of CFTR in health and disease. *J. Cyst. Fibros.* 6:1–14. <https://doi.org/10.1016/j.jcf.2006.09.002>
- Aoki, T., S. Ichimura, A. Itoh, M. Kuramoto, T. Shinkawa, T. Isobe, and M. Tagaya. 2009. Identification of the neuroblastoma-amplified gene product as a component of the syntaxin 18 complex implicated in Golgi-to-endoplasmic reticulum retrograde transport. *Mol. Biol. Cell.* 20: 2639–2649. <https://doi.org/10.1091/mbc.e08-11-1104>
- Appenzeller-Herzog, C., and H.P. Hauri. 2006. The ER-Golgi intermediate compartment (ERGIC): In search of its identity and function. *J. Cell Sci.* 119:2173–2183. <https://doi.org/10.1242/jcs.03019>
- Barr, F., and D.G. Lambright. 2010. Rab GEFs and GAPs. *Curr. Opin. Cell Biol.* 22:461–470. <https://doi.org/10.1016/j.ccb.2010.04.007>
- Blumer, J., J. Rey, L. Dehmelt, T. Mazel, Y.W. Wu, P. Bastiaens, R.S. Goody, and A. Itzen. 2013. RabGEFs are a major determinant for specific Rab membrane targeting. *J. Cell Biol.* 200:287–300. <https://doi.org/10.1083/jcb.201209113>
- Boncompain, G., N. Gareil, S. Tessier, A. Lescure, T.R. Jones, O. Kepp, G. Kroemer, E. Del Nery, and F. Perez. 2019. BML-265 and tyrphostin AG1478 disperse the Golgi apparatus and abolish protein transport in human cells. *Front. Cell Dev. Biol.* 7:232. <https://doi.org/10.3389/fcell.2019.00232>
- Bos, J.L., H. Rehmann, and A. Wittinghofer. 2007. GEFs and GAPs: Critical elements in the control of small G proteins. *Cell.* 129:865–877. <https://doi.org/10.1016/j.cell.2007.05.018>
- Brenner, S. 1974. The genetics of *Caenorhabditis elegans*. *Genetics.* 77:71–94. <https://doi.org/10.1093/genetics/77.1.71>

- Broeks, A., B. Gerrard, R. Allikmets, M. Dean, and R.H. Plasterk. 1996. Homologues of the human multidrug resistance genes MRP and MDR contribute to heavy metal resistance in the soil nematode *Caenorhabditis elegans*. *EMBO J.* 15:6132–6143
- Broeks, A., H.W. Janssen, J. Calafat, and R.H. Plasterk. 1995. A P-glycoprotein protects *Caenorhabditis elegans* against natural toxins. *EMBO J.* 14: 1858–1866
- Caplan, M.J. 1997. Membrane polarity in epithelial cells: Protein sorting and establishment of polarized domains. *Am. J. Physiol.* 272:F425–F429. <https://doi.org/10.1152/ajprenal.1997.272.4.F425>
- Chen, C.C.H., P.J. Schweinsberg, S. Vashist, D.P. Mareiniss, E.J. Lambie, and B.D. Grant. 2006. RAB-10 is required for endocytic recycling in the *Caenorhabditis elegans* intestine. *Mol. Biol. Cell.* 17:1286–1297. <https://doi.org/10.1091/mbc.e05-08-0787>
- Chen, D., C. Yang, S. Liu, W. Hang, X. Wang, J. Chen, and A. Shi. 2018. SAC-1 ensures epithelial endocytic recycling by restricting ARF-6 activity. *J. Cell Biol.* 217:2121–2139. <https://doi.org/10.1083/jcb.201711065>
- Collaco, A., R. Jakab, P. Hegan, M. Mooseker, and N. Ameen. 2010. Alpha-AP-2 directs myosin VI-dependent endocytosis of cystic fibrosis transmembrane conductance regulator chloride channels in the intestine. *J. Biol. Chem.* 285:17177–17187. <https://doi.org/10.1074/jbc.M110.127613>
- Cresawn, K.O., B.A. Potter, A. Oztan, C.J. Guerriero, G. Ihrke, J.R. Goldenring, G. Apodaca, and O.A. Weisz. 2007. Differential involvement of endocytic compartments in the biosynthetic traffic of apical proteins. *EMBO J.* 26:3737–3748. <https://doi.org/10.1038/sj.emboj.7601813>
- D'souza-Schorey, C., and P. Chavrier. 2006. ARF proteins: Roles in membrane traffic and beyond. *Nat. Rev. Mol. Cell Biol.* 7:347–358. <https://doi.org/10.1038/nrm1910>
- Debaixieux, S., F. Rayne, H. Yezid, and B. Beaumelle. 2012. The ins and outs of HIV-1 Tat. *Traffic.* 13:355–363. <https://doi.org/10.1111/j.1600-0854.2011.01286.x>
- Dierking, K., J. Polanowska, S. Omi, I. Engelmann, M. Gut, F. Lembo, J.J. Ewbank, and N. Pujol. 2011. Unusual regulation of a STAT protein by an SLC6 family transporter in *C. elegans* epidermal innate immunity. *Cell Host Microbe.* 9:425–435. <https://doi.org/10.1016/j.chom.2011.04.011>
- Dimou, E., and W. Nickel. 2010. Unconventional mechanisms of eukaryotic protein secretion. *Curr. Biol.* 28:R406–r410. <https://doi.org/10.1016/j.cub.2017.11.074>
- Ejlervskov, P., I. Rasmussen, T.T. Nielsen, A.L. Bergström, Y. Tohyama, P.H. Jensen, and F. Vilhardt. 2013. Tubulin polymerization-promoting protein (TPPP/p25 α) promotes unconventional secretion of α -synuclein through exophagy by impairing autophagosome-lysosome fusion. *J. Biol. Chem.* 288:17313–17335. <https://doi.org/10.1074/jbc.M112.401174>
- Engelmann, I., and N. Pujol. 2010. Innate immunity in *C. elegans*. *Adv. Exp. Med. Biol.* 708:105–121. https://doi.org/10.1007/978-1-4419-8059-5_6
- Folsch, H., P.E. Mattila, and O.A. Weisz. 2009. Taking the scenic route: Biosynthetic traffic to the plasma membrane in polarized epithelial cells. *Traffic.* 10:972–981. <https://doi.org/10.1111/j.1600-0854.2009.00927.x>
- Fourriere, L., A. Kasri, N. Gareil, S. Bardin, H. Bousquet, D. Pereira, F. Perez, B. Goud, G. Boncompain, and S. Miserey-Lenkei. 2019. RAB6 and microtubules restrict protein secretion to focal adhesions. *J. Cell Biol.* 218: 2215–2231. <https://doi.org/10.1083/jcb.201805002>
- Fromm, M.F. 2004. Importance of P-glycoprotein at blood-tissue barriers. *Trends Pharmacol. Sci.* 25:423–429. <https://doi.org/10.1016/j.tips.2004.06.002>
- Fu, D. 2013. Where is it and how does it get there: Intracellular localization and traffic of P-glycoprotein. *Front. Oncol.* 3:321. <https://doi.org/10.3389/fonc.2013.00321>
- Fuller, S.D., R. Bravo, and K. Simons. 1985. An enzymatic assay reveals that proteins destined for the apical or basolateral domains of an epithelial cell line share the same late Golgi compartments. *EMBO J.* 4:297–307
- Gee, H.Y., J. Kim, and M.G. Lee. 2018. Unconventional secretion of transmembrane proteins. *Semin. Cell Dev. Biol.* 83:59–66. <https://doi.org/10.1016/j.semcdb.2018.03.016>
- Gee, H.Y., S.H. Noh, B.L. Tang, K.H. Kim, and M.G. Lee. 2011. Rescue of Δ F508-CFTR trafficking via a GRASP-dependent unconventional secretion pathway. *Cell.* 146:746–760. <https://doi.org/10.1016/j.cell.2011.07.021>
- Giuliani, F., A. Grieve, and C. Rabouille. 2011. Unconventional secretion: A stress on GRASP. *Curr. Opin. Cell Biol.* 23:498–504. <https://doi.org/10.1016/j.cob.2011.04.005>
- Gleason, A.M., K.C.Q. Nguyen, D.H. Hall, and B.D. Grant. 2016. Syndapin/SDPN-1 is required for endocytic recycling and endosomal actin association in the *C. elegans* intestine. *Mol. Biol. Cell.* 27:3746–3756. <https://doi.org/10.1091/mbc.E16-02-0116>
- Gobel, V., P.L. Barrett, D.H. Hall, and J.T. Fleming. 2004. Lumen morphogenesis in *C. elegans* requires the membrane-cytoskeleton linker erm-1. *Dev. Cell.* 6:865–873. <https://doi.org/10.1016/j.devcel.2004.05.018>
- Grigoriev, I., K.L. Yu, E. Martinez-Sanchez, A. Serra-Marques, I. Smal, E. Meijering, J. Demmers, J. Peranen, R.J. Pasterkamp, P. Van Der Sluijs, et al. 2011. Rab6, Rab8, and MICAL3 cooperate in controlling docking and fusion of exocytotic carriers. *Curr. Biol.* 21:967–974. <https://doi.org/10.1016/j.cub.2011.04.030>
- Harada, A. 2010. Molecular mechanism of polarized transport. *J. Biochem.* 147: 619–624. <https://doi.org/10.1093/jb/mvq027>
- Hattula, K., J. Furuholm, A. Arffman, and J. Peranen. 2002. A Rab8-specific GDP/GTP exchange factor is involved in actin remodeling and polarized membrane transport. *Mol. Biol. Cell.* 13:3268–3280. <https://doi.org/10.1091/mbc.e02-03-0143>
- Hattula, K., J. Furuholm, J. Tikkanen, K. Tanhuanpaa, P. Laakkonen, and J. Peranen. 2006. Characterization of the Rab8-specific membrane traffic route linked to protrusion formation. *J. Cell Sci.* 119:4866–4877. <https://doi.org/10.1242/jcs.03275>
- Hoffmeister, H., K. Babinger, S. Gürster, A. Cedzich, C. Meese, K. Schandendorf, L. Osten, U. De Vries, A. Rasclé, and R. Witzgall. 2011. Polycystin-2 takes different routes to the somatic and ciliary plasma membrane. *J. Cell Biol.* 192:631–645. <https://doi.org/10.1083/jcb.201007050>
- Irazoqui, J.E., J.M. Urbach, and F.M. Ausubel. 2010. Evolution of host innate defense: Insights from *Caenorhabditis elegans* and primitive invertebrates. *Nat. Rev. Immunol.* 10:47–58. <https://doi.org/10.1038/nri2689>
- Jenkins, M.L., J.P. Margaria, J.T.B. Stariha, R.M. Hoffmann, J.A. Mcphail, D.J. Hamelin, M.J. Boulanger, E. Hirsch, and J.E. Burke. 2018. Structural determinants of Rab11 activation by the guanine nucleotide exchange factor SH3BP5. *Nat. Commun.* 9:3772. <https://doi.org/10.1038/s41467-018-06196-z>
- Jumper, J., R. Evans, A. Pritzel, T. Green, M. Figurnov, O. Ronneberger, K. Tunyasuvunakool, R. Bates, A. Zidek, A. Potapenko, et al. 2021. Highly accurate protein structure prediction with AlphaFold. *Nature.* 596: 583–589. <https://doi.org/10.1038/s41586-021-03819-2>
- Jung, J., J. Kim, S.H. Roh, I. Jun, R.D. Sampson, H.Y. Gee, J.Y. Choi, and M.G. Lee. 2016. The HSP70 co-chaperone DNAJC14 targets misfolded pendrin for unconventional protein secretion. *Nat. Commun.* 7:11386. <https://doi.org/10.1038/ncomms11386>
- Kamath, R.S., and J. Ahringer. 2003. Genome-wide RNAi screening in *Caenorhabditis elegans*. *Methods.* 30:313–321. [https://doi.org/10.1016/s1046-2023\(03\)00050-1](https://doi.org/10.1016/s1046-2023(03)00050-1)
- Kim, D.H., R. Feinbaum, G. Alloing, F.E. Emerson, D.A. Garsin, H. Inoue, M. Tanaka-Hino, N. Hisamoto, K. Matsumoto, M.W. Tan, and F.M. Ausubel. 2002. A conserved p38 MAP kinase pathway in *Caenorhabditis elegans* innate immunity. *Science.* 297:623–626. <https://doi.org/10.1126/science.1073759>
- Kim, J., H.Y. Gee, and M.G. Lee. 2018. Unconventional protein secretion: New insights into the pathogenesis and therapeutic targets of human diseases. *J. Cell Sci.* 131:jcs213686. <https://doi.org/10.1242/jcs.213686>
- Kim, J., S.H. Noh, H. Piao, D.H. Kim, K. Kim, J.S. Cha, W.Y. Chung, H.S. Cho, J.Y. Kim, and M.G. Lee. 2016. Monomerization and ER relocalization of GRASP is a requisite for unconventional secretion of CFTR. *Traffic.* 17: 733–753. <https://doi.org/10.1111/tra.12403>
- Klausner, R.D., J.G. Donaldson, and J. Lippincott-Schwartz. 1992. Brefeldin A: Insights into the control of membrane traffic and organelle structure. *J. Cell Biol.* 116:1071–1080. <https://doi.org/10.1083/jcb.116.5.1071>
- Kurz, C.L., M. Shapira, K. Chen, D.L. Baillie, and M.W. Tan. 2007. *Caenorhabditis elegans* pgp-5 is involved in resistance to bacterial infection and heavy metal and its regulation requires TIR-1 and a p38 map kinase cascade. *Biochem. Biophys. Res. Commun.* 363:438–443. <https://doi.org/10.1016/j.bbrc.2007.08.190>
- La Venuta, G., M. Zeitler, J.P. Steringer, H.M. Müller, and W. Nickel. 2015. The starting properties of fibroblast Growth factor 2: How to exit mammalian cells without a signal peptide at hand. *J. Biol. Chem.* 290: 27015–27020. <https://doi.org/10.1074/jbc.R115.689257>
- Lee, M.C.S., E.A. Miller, J. Goldberg, L. Orci, and R. Schekman. 2004. Bidirectional protein transport between the ER and Golgi. *Annu. Rev. Cell Dev. Biol.* 20:87–123. <https://doi.org/10.1146/annurev.cellbio.20.010403.105307>
- Li, W., P. Yi, and G. Ou. 2015. Somatic CRISPR-Cas9-induced mutations reveal roles of embryonically essential dynein chains in *Caenorhabditis elegans* cilia. *J. Cell Biol.* 208:683–692. <https://doi.org/10.1083/jcb.201411041>
- Lin, S.X., B. Grant, D. Hirsh, and F.R. Maxfield. 2001. Rme-1 regulates the distribution and function of the endocytic recycling compartment in

- mammalian cells. *Nat. Cell Biol.* 3:567–572. <https://doi.org/10.1038/35078543>
- Liu, H., S. Wang, W. Hang, J. Gao, W. Zhang, Z. Cheng, C. Yang, J. He, J. Zhou, J. Chen, and A. Shi. 2018. LET-413/Erbin acts as a RAB-5 effector to promote RAB-10 activation during endocytic recycling. *J. Cell Biol.* 217: 299–314. <https://doi.org/10.1083/jcb.201705136>
- Lock, R., C.M. Kenific, A.M. Leidal, E. Salas, and J. Debnath. 2014. Autophagy-dependent production of secreted factors facilitates oncogenic RAS-driven invasion. *Cancer Discov.* 4:466–479. <https://doi.org/10.1158/2159-8290.CD-13-0841>
- Longman, D., N. Hug, M. Keith, C. Anastasaki, E.E. Patton, G. Grimes, and J.F. Caceres. 2013. DHX34 and NBAS form part of an autoregulatory NMD circuit that regulates endogenous RNA targets in human cells, zebrafish and *Caenorhabditis elegans*. *Nucleic Acids Res.* 41:8319–8331. <https://doi.org/10.1093/nar/gkt585>
- Longman, D., R.H.A. Plasterk, I.L. Johnstone, and J.F. Caceres. 2007. Mechanistic insights and identification of two novel factors in the *C. elegans* NMD pathway. *Genes Dev.* 21:1075–1085. <https://doi.org/10.1101/gad.417707>
- Macqueen, A.J., J.J. Baggett, N. Perumov, R.A. Bauer, T. Januszewski, L. Schriefer, and J.A. Waddle. 2005. ACT-5 is an essential *Caenorhabditis elegans* actin required for intestinal microvilli formation. *Mol. Biol. Cell.* 16:3247–3259. <https://doi.org/10.1091/mbc.e04-12-1061>
- Mahajan-Miklos, S., M.W. Tan, L.G. Rahme, and F.M. Ausubel. 1999. Molecular mechanisms of bacterial virulence elucidated using a *Pseudomonas aeruginosa*-*Caenorhabditis elegans* pathogenesis model. *Cell.* 96: 47–56. [https://doi.org/10.1016/S0092-8674\(00\)80958-7](https://doi.org/10.1016/S0092-8674(00)80958-7)
- Malhotra, V. 2013. Unconventional protein secretion: An evolving mechanism. *EMBO J.* 32:1660–1664. <https://doi.org/10.1038/emboj.2013.104>
- Mcewan, D.L., A.S. Weisman, and C.P. Hunter. 2012. Uptake of extracellular double-stranded RNA by SID-2. *Mol. Cell.* 47:746–754. <https://doi.org/10.1016/j.molcel.2012.07.014>
- Mcgrath, J.P., and A. Varshavsky. 1989. The yeast STE6 gene encodes a homologue of the mammalian multidrug resistance P-glycoprotein. *Nature.* 340:400–404. <https://doi.org/10.1038/340400a0>
- Molinari, A., M. Cianfriglia, S. Meschini, A. Calcabrini, and G. Arancia. 1994. P-glycoprotein expression in the Golgi apparatus of multidrug-resistant cells. *Int. J. Cancer.* 59:789–795. <https://doi.org/10.1002/ijc.2910590614>
- Mouchiroud, L., L. Molin, P. Kasturi, M.N. Triba, M.E. Dumas, M.C. Wilson, A.P. Halestrap, M. Roussel, I. Masse, N. Dallière, et al. 2011. Pyruvate imbalance mediates metabolic reprogramming and mimics lifespan extension by dietary restriction in *Caenorhabditis elegans*. *Aging Cell.* 10: 39–54. <https://doi.org/10.1111/j.1474-9726.2010.00640.x>
- Muller, M.P., and R.S. Goody. 2018. Molecular control of Rab activity by GEFs, GAPs and GDI. *Small GTPases.* 9:5–21. <https://doi.org/10.1080/21541248.2016.1276999>
- Munro, S. 2011. The golgin coiled-coil proteins of the Golgi apparatus. *Cold Spring Harbor Perspect. Biol.* 3:a005256. <https://doi.org/10.1101/cshperspect.a005256>
- Nagai, T., K. Ibata, E.S. Park, M. Kubota, K. Mikoshiba, and A. Miyawaki. 2002. A variant of yellow fluorescent protein with fast and efficient maturation for cell-biological applications. *Nat. Biotechnol.* 20:87–90. <https://doi.org/10.1038/nbt0102-87>
- Nehrke, K. 2003. A reduction in intestinal cell pH_i due to loss of the *Caenorhabditis elegans* Na⁺/H⁺ exchanger NHX-2 increases life span. *J. Biol. Chem.* 278:44657–44666. <https://doi.org/10.1074/jbc.M307351200>
- Nelson, W.J., and C. Yeaman. 2001. Protein trafficking in the exocytic pathway of polarized epithelial cells. *Trends Cell Biol.* 11:483–486. [https://doi.org/10.1016/S0962-8924\(01\)02145-6](https://doi.org/10.1016/S0962-8924(01)02145-6)
- Noh, S.H., H.Y. Gee, Y. Kim, H. Piao, J. Kim, C.M. Kang, G. Lee, I. Mook-Jung, Y. Lee, J.W. Cho, and M.G. Lee. 2018. Specific autophagy and ESCRT components participate in the unconventional secretion of CFTR. *Autophagy.* 14:1761–1778. <https://doi.org/10.1080/15548627.2018.1489479>
- Pai, E.F., U. Krengel, G.A. Petsko, R.S. Goody, and A. Wittinghofer. 1990. Refined crystal structure of the triphosphate conformation of H-ras p21 at 1.35 Å resolution: Implications for the mechanism of GTP hydrolysis. *EMBO J.* 9:2351–2359
- Pan, H., J. Yu, L. Zhang, A. Carpenter, H. Zhu, L. Li, D. Ma, and J. Yuan. 2008. A novel small molecule regulator of guanine nucleotide exchange activity of the ADP-ribosylation factor and golgi membrane trafficking. *J. Biol. Chem.* 283:31087–31096. <https://doi.org/10.1074/jbc.M806592200>
- Park, H., D.H. Shin, J.R. Sim, S. Aum, and M.G. Lee. 2020. IRE1α kinase-mediated unconventional protein secretion rescues misfolded CFTR and pendrin. *Sci. Adv.* 6:eaax9914. <https://doi.org/10.1126/sciadv.aax9914>
- Piao, H., J. Kim, S.H. Noh, H.S. Kweon, J.Y. Kim, and M.G. Lee. 2017. Sec16A is critical for both conventional and unconventional secretion of CFTR. *Sci. Rep.* 7:39887. <https://doi.org/10.1038/srep39887>
- Pujol, N., S. Cypowyj, K. Ziegler, A. Millet, A. Astrain, A. Goncharov, Y. Jin, A.D. Chisholm, and J.J. Ewbank. 2008a. Distinct innate immune responses to infection and wounding in the *C. elegans* epidermis. *Curr. Biol.* 18:481–489. <https://doi.org/10.1016/j.cub.2008.02.079>
- Pujol, N., O. Zugasti, D. Wong, C. Couillault, C.L. Kurz, H. Schulenburg, and J.J. Ewbank. 2008b. Anti-fungal innate immunity in *C. elegans* is enhanced by evolutionary diversification of antimicrobial peptides. *PLoS Pathog.* 4:e1000105. <https://doi.org/10.1371/journal.ppat.1000105>
- Rabouille, C. 2017. Pathways of unconventional protein secretion. *Trends Cell Biol.* 27:230–240. <https://doi.org/10.1016/j.tcb.2016.11.007>
- Rabouille, C., V. Malhotra, and W. Nickel. 2012. Diversity in unconventional protein secretion. *J. Cell Sci.* 125:5251–5255. <https://doi.org/10.1242/jcs.103630>
- Roland, J.T., A.K. Kenworthy, J. Peranen, S. Caplan, and J.R. Goldenring. 2007. Myosin Vb interacts with Rab8a on a tubular network containing EHD1 and EHD3. *Mol. Biol. Cell.* 18:2828–2837. <https://doi.org/10.1091/mbc.e07-02-0169>
- Sakaguchi, A., M. Sato, K. Sato, K. Gengyo-Ando, T. Yorimitsu, J. Nakai, T. Hara, K. Sato, and K. Sato. 2015. REI-1 is a Guanine nucleotide exchange factor regulating RAB-11 localization and function in *C. elegans* embryos. *Dev. Cell.* 35:211–221. <https://doi.org/10.1016/j.devcel.2015.09.013>
- Sato, K., A. Norris, M. Sato, and B.D. Grant. 2014a. *C. elegans* as a Model for Membrane Traffic. *WormBook.* 1–47
- Sato, K., M. Sato, and A. Nakano. 2001. Rer1p, a retrieval receptor for endoplasmic reticulum membrane proteins, is dynamically localized to the Golgi apparatus by coatomer. *J. Cell Biol.* 152:935–944. <https://doi.org/10.1083/jcb.152.5.935>
- Sato, M., K. Saegusa, K. Sato, T. Hara, A. Harada, and K. Sato. 2011. *Caenorhabditis elegans* SNAP-29 is required for organellar integrity of the endomembrane system and general exocytosis in intestinal epithelial cells. *Mol. Biol. Cell.* 22:2579–2587. <https://doi.org/10.1091/mbc.E11-04-0279>
- Sato, M., K. Sato, P. Fonarev, C.J. Huang, W. Liou, and B.D. Grant. 2005. *Caenorhabditis elegans* RME-6 is a novel regulator of RAB-5 at the clathrin-coated pit. *Nat. Cell Biol.* 7:559–569. <https://doi.org/10.1038/ncb1261>
- Sato, M., K. Sato, W. Liou, S. Pant, A. Harada, and B.D. Grant. 2008. Regulation of endocytic recycling by *C. elegans* Rab35 and its regulator RME-4, a coated-pit protein. *EMBO J.* 27:1183–1196. <https://doi.org/10.1038/emboj.2008.54>
- Sato, T., T. Iwano, M. Kunii, S. Matsuda, R. Mizuguchi, Y. Jung, H. Hagiwara, Y. Yoshihara, M. Yuzaki, R. Harada, and A. Harada. 2014b. Rab8a and Rab8b are essential for several apical transport pathways but insufficient for ciliogenesis. *J. Cell Sci.* 127:422–431. <https://doi.org/10.1242/jcs.136903>
- Sato, T., S. Mushiaki, Y. Kato, K. Sato, M. Sato, N. Takeda, K. Ozono, K. Miki, Y. Kubo, A. Tsuji, et al. 2007. The Rab8 GTPase regulates apical protein localization in intestinal cells. *Nature.* 448:366–369. <https://doi.org/10.1038/nature05929>
- Schapiro, M., M. Tyers, M. Torrent, and C.H. Arrowsmith. 2017. WD40 repeat domain proteins: A novel target class? *Nat. Rev. Drug Dis.* 16:773–786. <https://doi.org/10.1038/nrd.2017.179>
- Schmitt, H.D. 2010. Dsl1p/Zw10: Common mechanisms behind tethering vesicles and microtubules. *Trends Cell Biol.* 20:257–268. <https://doi.org/10.1016/j.tcb.2010.02.001>
- Schotman, H., L. Karhinen, and C. Rabouille. 2008. dGRASP-mediated non-canonical integrin secretion is required for *Drosophila* epithelial remodeling. *Dev. Cell.* 14:171–182. <https://doi.org/10.1016/j.devcel.2007.12.006>
- Schröder, M., and R.J. Kaufman. 2005. The mammalian unfolded protein response. *Annu. Rev. Biochem.* 74:739–789. <https://doi.org/10.1146/annurev.biochem.73.011303.074134>
- Sheff, D.R., R. Kroschewski, and I. Mellman. 2002. Actin dependence of polarized receptor recycling in Madin-Darby canine kidney cell endosomes. *Mol. Biol. Cell.* 13:262–275. <https://doi.org/10.1091/mbc.01-07-0320>
- Shen, Z., X. Zhang, Y. Chai, Z. Zhu, P. Yi, G. Feng, W. Li, and G. Ou. 2014. Conditional knockouts generated by engineered CRISPR-Cas9 endonuclease reveal the roles of coronin in *C. elegans* neural development. *Dev. Cell.* 30:625–636. <https://doi.org/10.1016/j.devcel.2014.07.017>
- Sheps, J.A., S. Ralph, Z. Zhao, D.L. Baillie, and V. Ling. 2004. The ABC transporter gene family of *Caenorhabditis elegans* has implications for

- the evolutionary dynamics of multidrug resistance in eukaryotes *Genome Biol.* 5:R15. <https://doi.org/10.1186/gb-2004-5-3-r15>
- Shi, A., C.C.H. Chen, R. Banerjee, D. Glodowski, A. Audhya, C. Rongo, and B.D. Grant. 2010. EHBP-1 functions with RAB-10 during endocytic recycling in *Caenorhabditis elegans*. *Mol. Biol. Cell.* 21:2930–2943. <https://doi.org/10.1091/mbc.E10-02-0149>
- Son, S.M., M.Y. Cha, H. Choi, S. Kang, H. Choi, M.S. Lee, S.A. Park, and I. Mook-Jung. 2016. Insulin-degrading enzyme secretion from astrocytes is mediated by an autophagy-based unconventional secretory pathway in Alzheimer disease. *Autophagy.* 12:784–800. <https://doi.org/10.1080/15548627.2016.1159375>
- Steinberg, F., K.J. Heesom, M.D. Bass, and P.J. Cullen. 2012. SNX17 protects integrins from degradation by sorting between lysosomal and recycling pathways. *J. Cell Biol.* 197:219–230. <https://doi.org/10.1083/jcb.201111121>
- Steinfeld, N., V. Lahiri, A. Morrison, S.P. Metur, D.J. Klionsky, and L.S. Weisman. 2021. Elevating PI3P drives select downstream membrane trafficking pathways. *Mol. Biol. Cell.* 32:143–156. <https://doi.org/10.1091/mbc.E20-03-0191>
- Steringer, J.P., H.M. Müller, and W. Nickel. 2015. Unconventional secretion of fibroblast growth factor 2: A novel type of protein translocation across membranes? *J. Mol. Biol.* 427:1202–1210. <https://doi.org/10.1016/j.jmb.2014.07.012>
- Tagaya, M., K. Arasaki, H. Inoue, and H. Kimura. 2014. Moonlighting functions of the NRZ (mammalian Dsl1) complex. *Front. Cell Dev. Biol.* 2:25. <https://doi.org/10.3389/fcell.2014.00025>
- Tan, M.W., S. Mahajan-Miklos, and F.M. Ausubel. 1999a. Killing of *Caenorhabditis elegans* by *Pseudomonas aeruginosa* used to model mammalian bacterial pathogenesis. *Proc. Natl. Acad. Sci. USA.* 96:715–720. <https://doi.org/10.1073/pnas.96.2.715>
- Tan, M.W., L.G. Rahme, J.A. Sternberg, R.G. Tompkins, and F.M. Ausubel. 1999b. *Pseudomonas aeruginosa* killing of *Caenorhabditis elegans* used to identify *P. aeruginosa* virulence factors. *Proc. Natl. Acad. Sci. USA.* 96:2408–2413. <https://doi.org/10.1073/pnas.96.5.2408>
- Tanaka, A.R., F. Kano, K. Ueda, and M. Murata. 2008. The ABCA1 Q597R mutant undergoes trafficking from the ER upon ER stress. *Biochem. Biophys. Res. Commun.* 369:1174–1178. <https://doi.org/10.1016/j.bbrc.2008.03.018>
- Thuenaer, R., Y.C. Hsu, J.M. Carvajal-Gonzalez, S. Deborde, J.Z. Chuang, W. Romer, A. Sonnleitner, E. Rodriguez-Boulan, and C.H. Sung. 2014. Four-dimensional live imaging of apical biosynthetic trafficking reveals a post-Golgi sorting role of apical endosomal intermediates. *Proc. Natl. Acad. Sci. USA.* 111:4127–4132. <https://doi.org/10.1073/pnas.1304168111>
- Tian, G., P. Ropelewski, I. Nemet, R. Lee, K.H. Lodowski, and Y. Imanishi. 2014. An unconventional secretory pathway mediates the cilia targeting of peripherin/rds. *J. Neurosci.* 34:992–1006. <https://doi.org/10.1523/JNEUROSCI.3437-13.2014>
- Tian, Y., Q. Kang, X. Shi, Y. Wang, N. Zhang, H. Ye, Q. Xu, T. Xu, and R. Zhang. 2021. SNX-3 mediates retromer-independent tubular endosomal recycling by opposing EEA-1-facilitated trafficking. *PLoS Genet.* 17:e1009607. <https://doi.org/10.1371/journal.pgen.1009607>
- Timmons, L., and A. Fire. 1998. Specific interference by ingested dsRNA. *Nature.* 395:854. <https://doi.org/10.1038/27579>
- Varadi, M., S. Anyango, M. Deshpande, S. Nair, C. Natassia, G. Yordanova, D. Yuan, O. Stroe, G. Wood, A. Laydon, et al. 2022. AlphaFold protein structure database: Massively expanding the structural coverage of protein-sequence space with high-accuracy models. *Nucleic Acids Res.* 50:D439–D444. <https://doi.org/10.1093/nar/gkab1061>
- Vogel, G.F., K.M.C. Klee, A.R. Janecke, T. Muller, M.W. Hess, and L.A. Huber. 2015. Cargo-selective apical exocytosis in epithelial cells is conducted by Myo5B, Slp4a, Vamp7, and Syntaxin 3. *J. Cell Biol.* 211:587–604. <https://doi.org/10.1083/jcb.201506112>
- Wang, P., H. Liu, Y. Wang, O. Liu, J. Zhang, A. Gleason, Z. Yang, H. Wang, A. Shi, and B.D. Grant. 2016. RAB-10 promotes EHBP-1 bridging of filamentous actin and tubular recycling endosomes. *PLoS Genet.* 12:e1006093. <https://doi.org/10.1371/journal.pgen.1006093>
- Winter, J.F., S. Hopfner, K. Korn, B.O. Farnung, C.R. Bradshaw, G. Marsico, M. Volkmer, B. Habermann, and M. Zerial. 2012. *Caenorhabditis elegans* screen reveals role of PAR-5 in RAB-11-recycling endosome positioning and apical cell polarity. *Nat. Cell Biol.* 14:666–676. <https://doi.org/10.1038/ncb2508>
- Woldemichael, G.M., T.J. Turbyville, W.M. Linehan, and J.B. McMahon. 2011. Carminomycin I is an apoptosis inducer that targets the Golgi complex in clear cell renal carcinoma cells. *Cancer Res.* 71:134–142. <https://doi.org/10.1158/0008-5472.CAN-10-0757>
- Yamamoto, T.G., S. Watanabe, A. Essex, and R. Kitagawa. 2008. SPDL-1 functions as a kinetochore receptor for MDF-1 in *Caenorhabditis elegans*. *J. Cell Biol.* 183:187–194. <https://doi.org/10.1083/jcb.200805185>
- Yoo, J.S., B.D. Moyer, S. Bannykh, H.M. Yoo, J.R. Riordan, and W.E. Balch. 2002. Non-conventional trafficking of the cystic fibrosis transmembrane conductance regulator through the early secretory pathway. *J. Biol. Chem.* 277:11401–11409. <https://doi.org/10.1074/jbc.M110263200>
- Zeitler, M., J.P. Steringer, H.M. Müller, M.P. Mayer, and W. Nickel. 2015. HIV-tat protein forms phosphoinositide-dependent membrane pores implicated in unconventional protein secretion. *J. Biol. Chem.* 290:21976–21984. <https://doi.org/10.1074/jbc.M115.667097>
- Zhang, M., L. Liu, X. Lin, Y. Wang, Y. Li, Q. Guo, S. Li, Y. Sun, X. Tao, D. Zhang, et al. 2020. A translocation pathway for vesicle-mediated unconventional protein secretion. *Cell.* 181:637–652.e15. <https://doi.org/10.1016/j.cell.2020.03.031>
- Zhang, M., and R. Schekman. 2013. Cell biology. Unconventional secretion, unconventional solutions. *Science.* 340:559–561. <https://doi.org/10.1126/science.1234740>

Supplemental material

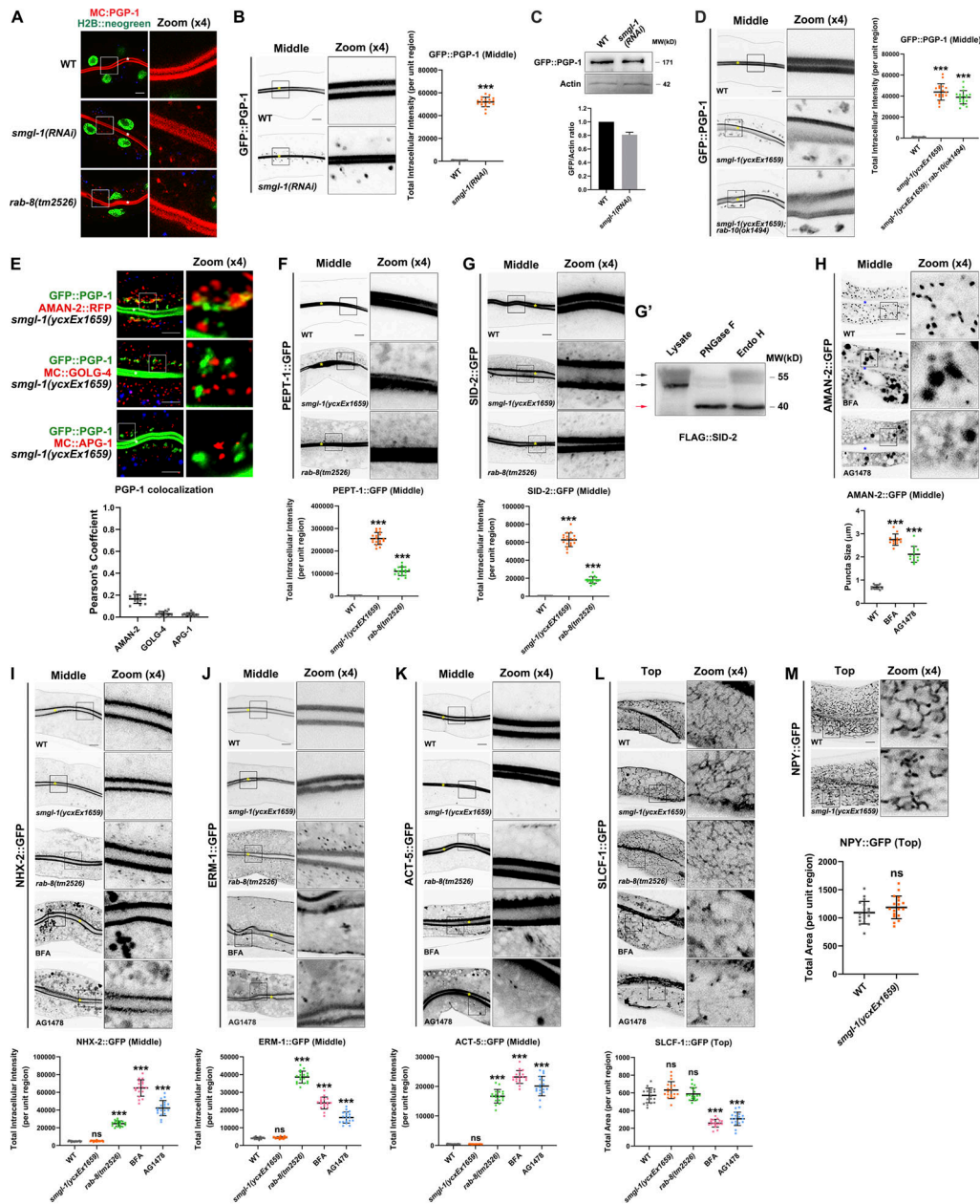


Figure S1. Loss of RAB-8 leads to the aberrant distribution of all apical but not basolateral proteins, and BFA or AG1478 treatment impairs the intracellular distribution of AMAN-2, NHX-2, ERM-1, ACT-5, and SLCF-1. (A) Confocal images showing the intracellular localization pattern of PGP-1 in *smgl-1* and *rab-8* deficient animals, using H2B::neogreen as a nuclear marker. (B) GFP::PGP-1 accumulated in intracellular structures in SMGL-1 knockdown animals. (C) Expressional levels of GFP::PGP-1 in wild-type and SMGL-1 knockdown animals. (D) The distributional defects of PGP-1 in *smgl-1* mutants were not exacerbated by simultaneous loss of RAB-10. (E) GFP::PGP-1-labeled puncta were separable from Golgi markers AMAN-2::RFP (cis- and medial-Golgi cisternae), mCherry::GOLG-4 (TGN), and mCherry::APG-1 (TGN) in *smgl-1(yxcx1659)* mutants. Pearson's correlation coefficients for GFP and mCherry signals were calculated ($n = 12$ animals). The signals from the apical membrane were avoided by manual ROI selection. (F and G) PEPT-1::GFP and SID-2::GFP accumulated in intracellular structures in *smgl-1(yxcx1659)* and *rab-8(tm2526)* mutants. (G') FLAG::SID-2 transgenic animals were analyzed by immunoblotting using anti-FLAG antibody after Endo H or PNGase F treatment. (H) BFA and AG1478 treatment disrupted the intracellular localization of AMAN-2::GFP. (I-K) The localization of NHX-2::GFP, ERM-1::GFP, and ACT-5::GFP remained unchanged in *smgl-1(yxcx1659)* but accumulated on intracellular structures and/or basolateral membrane in *rab-8(tm2526)* mutants. BFA and AG1478 treatment caused the intracellular accumulation of NHX-2::GFP, ERM-1::GFP, and ACT-5::GFP. (L) The basolateral membrane protein SLCF-1::GFP exhibited similar tubular localization in wild-type, *smgl-1(yxcx1659)*, and *rab-8(tm2526)* mutants. BFA and AG1478 treatment disrupted SLCF-1::GFP-labeled basolateral tubular structures. (M) The basolateral membrane protein NPY::GFP exhibited similar tubular localization in wild-type, *smgl-1(yxcx1659)*, and *rab-8(tm2526)* mutants. The signals from the apical membrane were avoided by manual ROI selection. Data are shown as mean \pm SD ($n = 18$ each, six animals of each genotype sampled in three different unit regions of each intestine defined by a 100×100 [pixel²] box positioned at random). Statistical significance was determined using a two-tailed, unpaired Student's *t* test. For multiple comparisons, statistical significance was determined using a one-way ANOVA followed by a post-hoc test (Dunn's Multiple Comparison Test). ***, $P < 0.001$. Data distribution was assumed to be normal, but this was not formally tested. Scale bars: 10 μ m. Colored asterisks indicate intestinal lumen. A dotted line indicates the outline of the intestine. Source data are available for this figure: SourceData FS1.

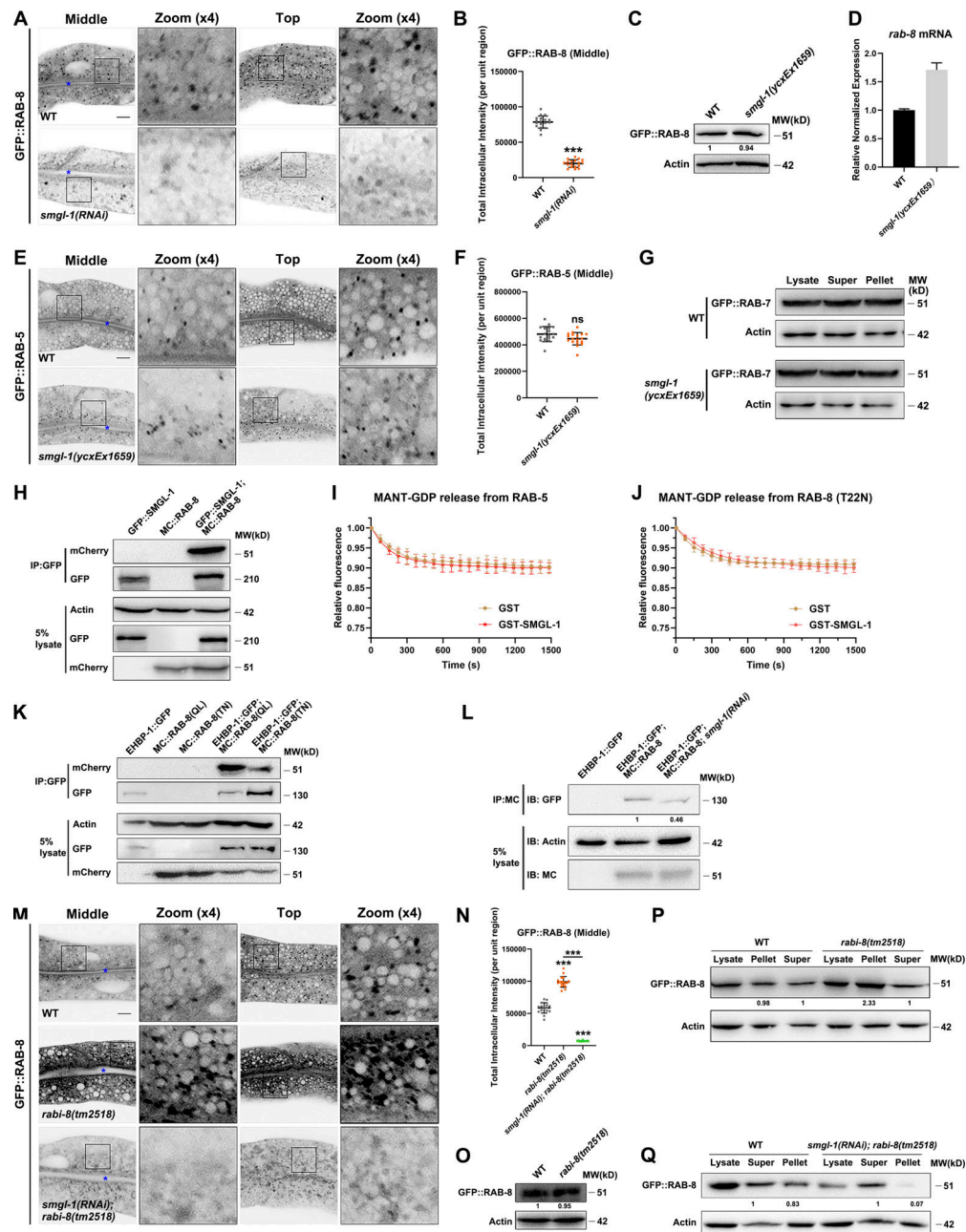


Figure S2. SMGL-1 interacts with RAB-8 and acts as a guanine nucleotide exchange factor for RAB-8. (A and B) Confocal images of intestinal cells expressing GFP-tagged RAB-8. SMGL-1 knockdown reduced the number of GFP::RAB-8-labeled puncta. **(C)** Expression level of GFP::RAB-8 in wild-type and *smgl-1(ycxEx1659)* animals. **(D)** Levels of *rab-8* mRNA in wild-type and *smgl-1(ycxEx1659)* animals. Each is the average of three replicates. **(E and F)** The intracellular distribution of GFP::RAB-5 did not change in *smgl-1(ycxEx1659)* mutants. **(G)** Western blot showing GFP-tagged RAB-7 in worm lysate, supernatant and pellet. The membrane-to-cytosol (pellet-to-supernatant) ratio of GFP::RAB-7 (late endosome marker) was not affected by SMGL-1 knockout. **(H)** In a co-IP assay, GFP::SMGL-1 precipitated with MC::RAB-8. **(I and J)** In vitro GEF assay. MANT-GDP release from RAB-5 or RAB-8(T22N) was not facilitated by adding GST-SMGL-1. **(K)** In a co-IP assay, EHBP-1::GFP preferentially precipitated with MC::RAB-8(Q67L). **(L)** EHBP-1::GFP co-immunoprecipitated by MC::RAB-8 were reduced in SMGL-1 knockdown animals. Levels of EHBP-1::GFP were normalized to the corresponding actin (set to one in wild-type animals). **(M and N)** The intensity of GFP::RAB-8 was increased in *rabi-8(tm2518)* and reduced in *smgl-1(RNAi); rabi-8(tm2518)* animals. The signals from the apical membrane were avoided by manual ROI selection. Data are shown as mean \pm SD ($n = 18$ each, six animals of each genotype sampled in three different unit regions of each intestine defined by a 100×100 [pixel²] box positioned at random). Statistical significance was determined using a two-tailed, unpaired Student's *t* test. For multiple comparisons, statistical significance was determined using a one-way ANOVA followed by a post-hoc test (Dunn's Multiple Comparison Test). ***, $P < 0.001$. Data distribution was assumed to be normal, but this was not formally tested. Scale bars: 10 μ m. Colored asterisks indicate intestinal lumen. A dotted line indicates the outline of the intestine. **(O)** The expression level of GFP::RAB-8 remained intact in *rabi-8(tm2518)* mutants. **(P)** The membrane-to-cytosol ratio of GFP::RAB-8 increased in *rabi-8(tm2518)* mutants. Actin served as the loading control. Levels of RAB-8 were normalized to the corresponding controls and set to one in the supernatant fraction. **(Q)** The membrane-to-cytosol ratio of GFP::RAB-8 decreased in *smgl-1(RNAi); rabi-8(tm2518)* animals. Actin served as the loading control. Levels of RAB-8 were normalized to the corresponding controls and set to one in the supernatant fraction. Source data are available for this figure: SourceData FS2.

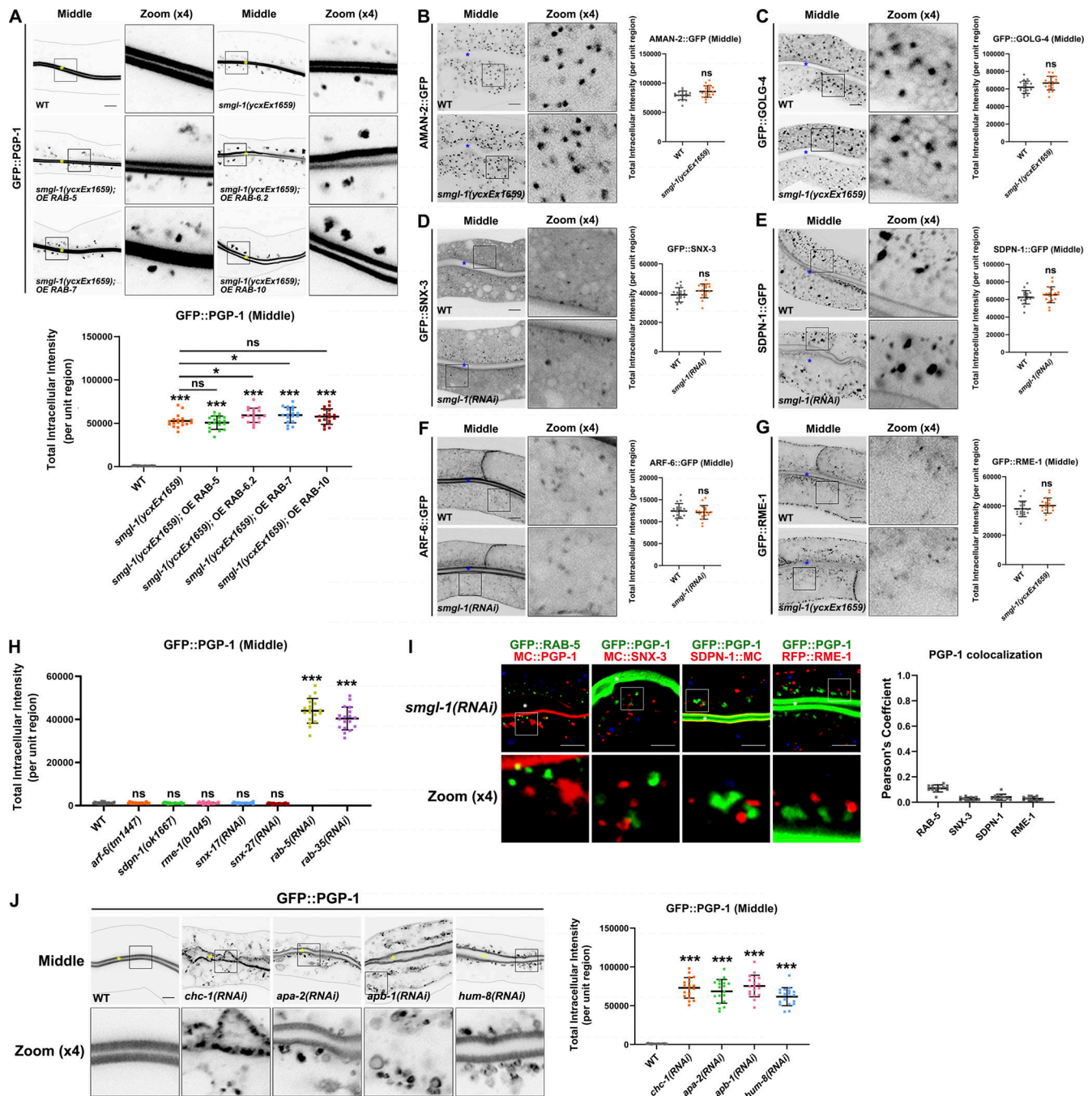


Figure S3. **The apical secretion defects of PGP-1 in *smgl-1* mutants are not due to the deficiency of other Rabs, impaired Golgi integrity, or recycling transport.** (A) Overexpression of RAB-5, RAB-6.2, RAB-7 and RAB-10 failed to rescue the localization defects of PGP-1 in *smgl-1(yex1659)* mutants. (B and C) The intracellular localization of AMAN-2::GFP and GFP::GOLG-4 remained intact in *smgl-1(yex1659)* mutants. (D–G) SMGL-1 deficiency did not affect the localization of recycling regulators SNX-3 (D), SDPN-1 (E), ARF-6 (F) or RME-1 (G). (H) PGP-1 did not accumulate in intracellular structures in animals lacking ARF-6, SDPN-1, RME-1, SNX-17 or SNX-27. However, there was a prominent PGP-1 accumulation in RAB-5 and RAB-35 knockdown animals. (I) In *smgl-1* knockdown animals, accumulated PGP-1 showed little colocalization with RAB-5 (early endosome), SDPN-1 (early and recycling endosome), SNX-3 (early and recycling endosome), and RME-1 (recycling endosome). Pearson's correlation coefficients for GFP and mCherry signals were calculated ($n = 12$ animals). The signals from the apical membrane were avoided by manual ROI selection. (J) CHC-1 knockdown led to the aggregation of PGP-1 in the apical membrane. Knockdown of APA-2 and APB-1 caused the ring-like structures of PGP-1 beneath the membranes. Knockdown of HUM-8 resulted in similar subapical ring-like structures. The signals from the apical membrane were avoided by manual ROI selection. Data are shown as mean \pm SD ($n = 18$ each, six animals of each genotype sampled in three different unit regions of each intestine defined by a 100×100 [pixel²] box positioned at random). Statistical significance was determined using a two-tailed, unpaired Student's *t* test. For multiple comparisons, statistical significance was determined using a one-way ANOVA followed by a post-hoc test (Dunn's Multiple Comparison Test). *, $P < 0.05$; ***, $P < 0.001$. Data distribution was assumed to be normal, but this was not formally tested. Scale bars: 10 μ m. Colored asterisks indicate intestinal lumen. A dotted line indicates the outline of the intestine.

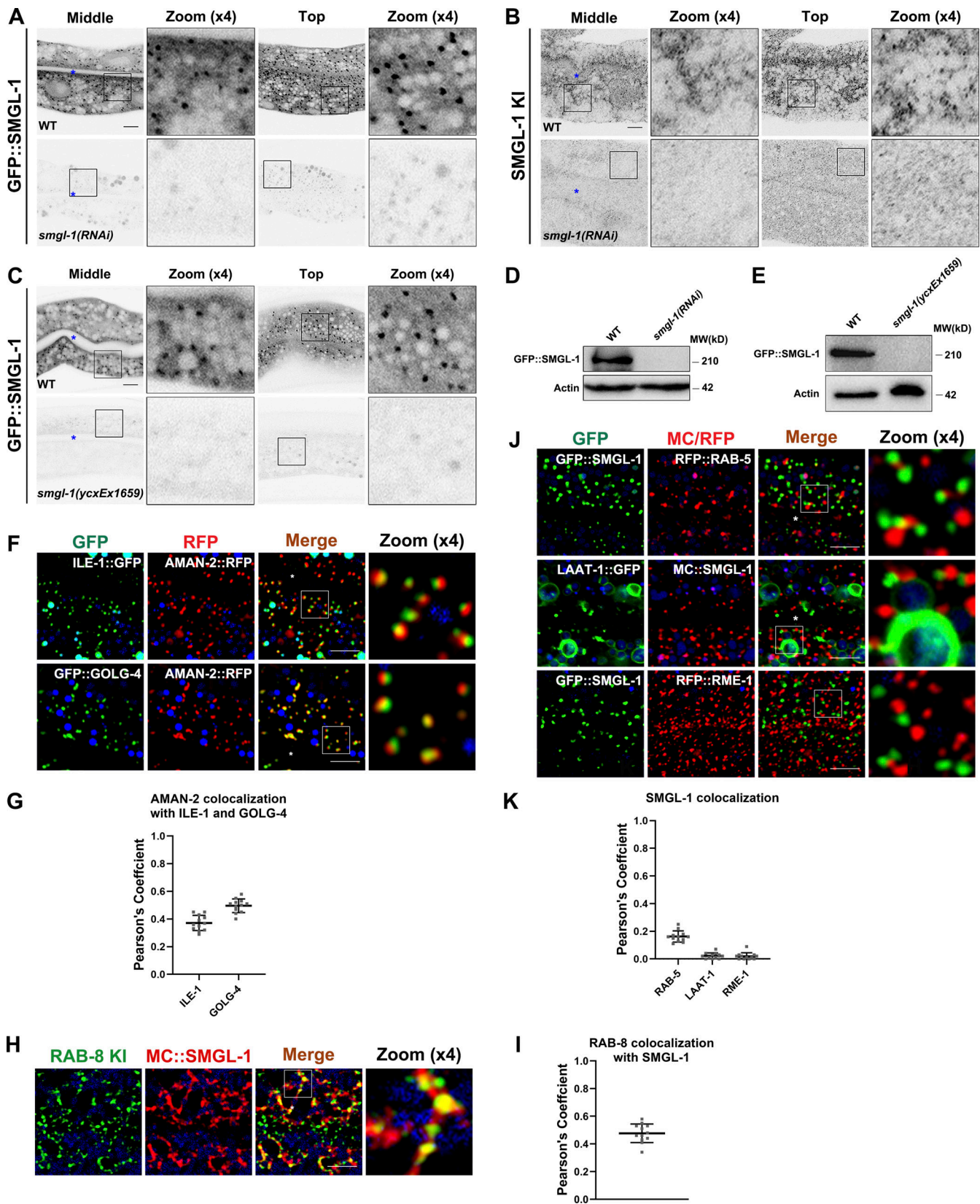


Figure S4. **SMGL-1 resides in the ER-Golgi intermediate compartment and neighboring RAB-8-positive structures. (A–E)** In *smgl-1(RNAi)* animals or *smgl-1(ycxEx1659)* mutants, the expression levels of GFP::SMGL-1 and endogenous SMGL-1 were decreased. **(F and G)** The intracellular juxtaposition between AMAN-2 and ILE-1 or GOLG-4. **(H and I)** Endogenous RAB-8 colocalized with MC::SMGL-1. **(J and K)** SMGL-1-positive puncta were separable from RAB-5, LAAT-1, and RME-1. Pearson's correlation coefficients for GFP and mCherry signals were calculated ($n = 12$ animals). The signals from the apical membrane were avoided by manual ROI selection. Scale bars: 10 μm . Colored asterisks indicate intestinal lumen. Source data are available for this figure: SourceData FS4.

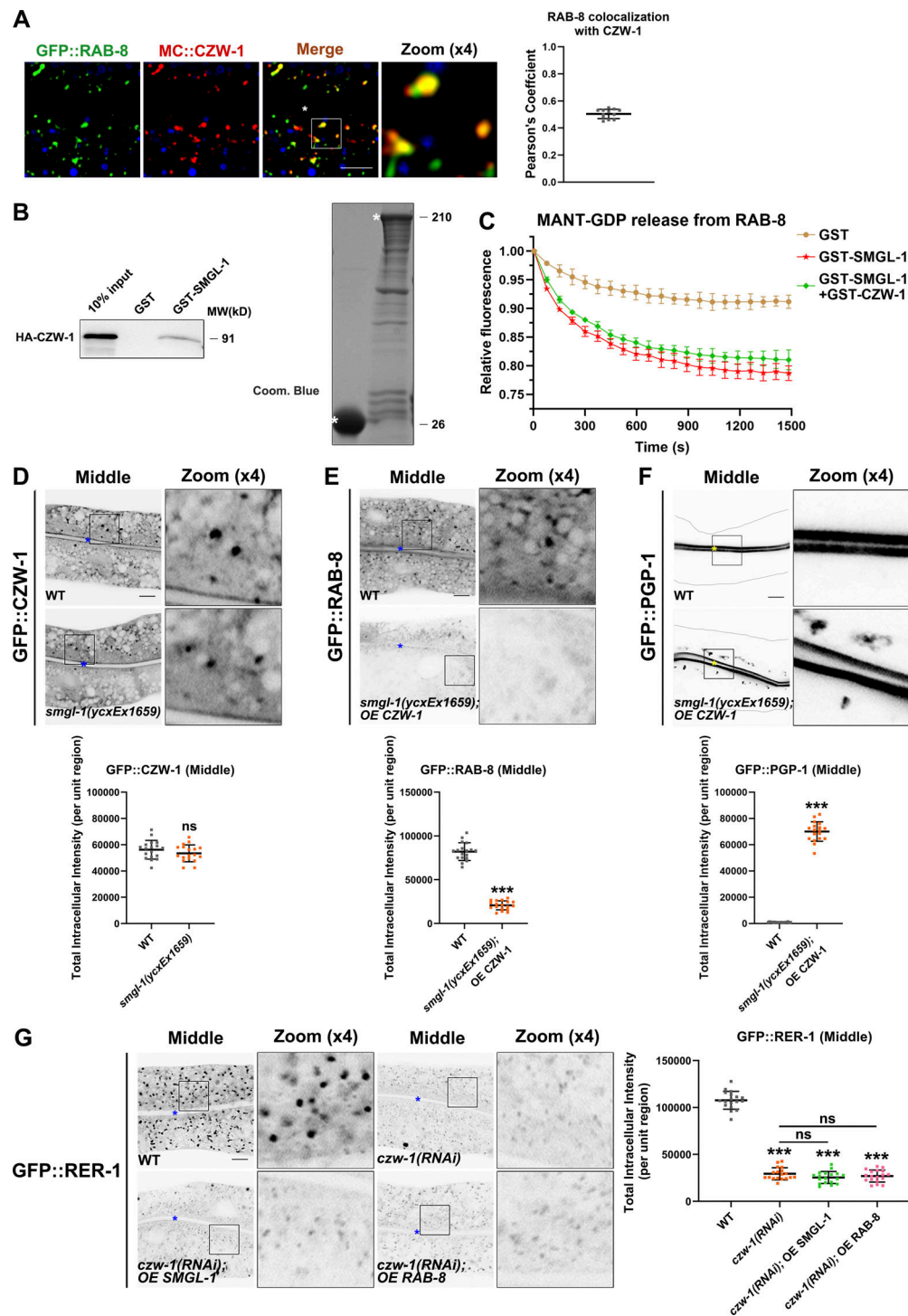


Figure S5. **CZW-1 interacts with SMGL-1 and promotes the subcellular localization of SMGL-1.** (A) CZW-1 colocalized with a subset of RAB-8-positive endosomal structures. Pearson's correlation coefficients for GFP and mCherry signals were calculated ($n = 12$ animals). The signals from the apical membrane were avoided by manual ROI selection. (B) GST-SMGL-1 pulled down HA-CZW-1 in an in vitro pull-down assay. (C) In vitro GEF assay. MANT-GDP release from RAB-8 was measured by adding GST-only, GST-SMGL-1, and GST-SMGL-1&GST-CZW-1. (D) The intracellular distribution of GFP::CZW-1 was not affected in *smgl-1(ycxEx1659)* mutants. (E and F) Overexpression of CZW-1 failed to rescue the localization defects of RAB-8 and PGP-1 in *smgl-1(ycxEx1659)* mutants. (G) GFP::RER-1 was diffusive and labeled dispersed small puncta in CZW-1 knockdown animals. Overexpression of SMGL-1 or RAB-8 failed to rescue the localization defects of GFP::RER-1. The signals from the apical membrane were avoided by manual ROI selection. Data are shown as mean \pm SD ($n = 18$ each, six animals of each genotype sampled in three different unit regions of each intestine defined by a 100×100 [pixel²] box positioned at random). Statistical significance was determined using a two-tailed, unpaired Student's *t* test. For multiple comparisons, statistical significance was determined using a one-way ANOVA followed by a post-hoc test (Dunn's Multiple Comparison Test). ***, $P < 0.001$. Data distribution was assumed to be normal, but this was not formally tested. Scale bars: 10 μ m. Colored asterisks indicate intestinal lumen. A dotted line indicates the outline of the intestine. Source data are available for this figure: SourceData F55.

Provided online are Table S1 and Table S2. Table S1 is a key resources table. Table S2 lists primers used in the study.